AWARD NUMBER: W81XWH-18-1-0805

TITLE: Macrophage Migration Inhibitor (MIF) Therapeutics for Neuroprotection and Prevention of Scar in Traumatic Retinal Detachment

PRINCIPAL INVESTIGATOR: Colleen Cebulla

CONTRACTING ORGANIZATION: Ohio State University, Columbus, OH

REPORT DATE: October 2021

TYPE OF REPORT: Annual Report

PREPARED FOR: U.S. Army Medical Research and Materiel Command
Fort Detrick, Maryland 21702-5012

REPORT DOCUMENTATION PAGE

Form Approved
OMB No. 0704-0188

1. REPORT DATE	**2. REPORT TYPE**	**3. DATES COVERED**
October 2021	Annual Report	30Sep2020-29Sep2021

4. TITLE AND SUBTITLE

Macrophage Migration Inhibitor (MIF) Therapeutics for Neuroprotection and Prevention of Scar in Traumatic Retinal Detachment

5a. CONTRACT NUMBER
W81XWH-18-1-0805

5b. GRANT NUMBER
W81XWH-18-1-0805

5c. PROGRAM ELEMENT NUMBER

6. AUTHOR(S): Colleen Cebulla, Elizabeth Urbanski, Tyler Heisler-Taylor, Sumaya Hamadmad

E-Mail: colleen.cebulla@osumc.edu

5d. PROJECT NUMBER
0011187957-0001

5e. TASK NUMBER

5f. WORK UNIT NUMBER

7. PERFORMING ORGANIZATION NAME(S) AND ADDRESS(ES)

The Ohio State University
1960 Kenny Road
Columbus, OH 43210-1016

8. PERFORMING ORGANIZATION REPORT NUMBER

9. SPONSORING / MONITORING AGENCY NAME(S) AND ADDRESS(ES)

U.S. Army Medical Research and Development Command
Fort Detrick, Maryland 21702-5012

10. SPONSOR/MONITOR'S ACRONYM(S)

11. SPONSOR/MONITOR'S REPORT NUMBER(S)

12. DISTRIBUTION / AVAILABILITY STATEMENT

Approved for Public Release; Distribution Unlimited

13. SUPPLEMENTARY NOTES

14. ABSTRACT

Retinal detachment (RD) is a prevalent cause of blindness that is common after ocular injury to military personnel. Permanent vision loss occurs due to death of photoreceptors and formation of excessive scar tissue, known as proliferative vitreoretinopathy (PVR). There are no effective pharmaceuticals to prevent these problems. The inflammatory protein, macrophage migration inhibitory factor (MIF), is produced at high levels in RD and PVR, as well as in excitotoxic (NMDA-mediated) damage, which is important in blast injury. The proposed research will test the ability of different clinically-relevant MIF inhibitors to block photoreceptor death and abnormal healing after RD or NMDA damage in different animal models. One of these drugs, ibudilast, has already been approved for human use in Japan as an anti-inflammatory agent and is currently undergoing clinical trials in the US as a neuroprotective agent for several neurologic diseases. This research will have considerable promise for treating ocular disease triggered by military injuries. We hope it will provide ground work for a clinical trial in patients, which could one day lead to therapeutics that could prevent vision loss.

15. SUBJECT TERMS
Retinal detachment (RD), proliferative vitreoretinopathy (PVR), N-methyl-D-aspartate (NMDA), macrophage migration inhibitory factor (MIF), MIF inhibitor, chick, rabbit, retinal pigment epithelium (RPE), ARPE-19, ibudilast, AV411, CPSI-1306, AV1013, scratch assay, MTT assay, contraction assay, epithelial mesenchymal transition (EMT)

16. SECURITY CLASSIFICATION OF:			**17. LIMITATION OF ABSTRACT**	**18. NUMBER OF PAGES**	**19a. NAME OF RESPONSIBLE PERSON**
a. REPORT	**b. ABSTRACT**	**c. THIS PAGE**			USAMRMC
Unclassified	Unclassified	Unclassified	Unclassified	40	**19b. TELEPHONE NUMBER** *(include area code)*

TABLE OF CONTENTS

1. INTRODUCTION:

Our project pertains to the FY17 VRP Technology/Therapeutic Development Award Focus Areas: “Preclinical animal studies to evaluate safety and/or efficacy of treatments or technologies returning form and function after traumatic injury to: (1) orbit and ocular tissues (optic nerve, retina, and uvea), (2) eyelid, and/or (3) adnexal structures” and “Preclinical animal studies to evaluate safety and/or efficacy of treatments or technologies to reduce/control scarring and/or pathological healing response(s) after military-relevant ocular/visual system injury.” Since MIF promotes photoreceptor apoptosis and retinal gliosis and it antagonizes the anti-inflammatory effects of glucocorticoids, which are the standard pharmacologic treatment used in traumatized eyes, our hypothesis is that clinically relevant MIF inhibitors that target the inflammatory response will yield benefit in retinal neuroprotection and scar prevention in traumatic retinal damage. Our hypothesis will be tested with the following specific aims. Aim 1: Test the hypothesis that clinically-relevant MIF inhibitors block neuronal apoptosis in our in vivo RD and NMDA damage models. We will evaluate neuroprotection using electrophysiology, spectral domain OCT (SD-OCT), fundus imaging, and histology. Any potential toxicity will be evaluated. Aim 2: Test the hypothesis that clinically-relevant MIF inhibitors block gliosis and pathologic wound healing in traumatic RD. Studies with cell lines (retinal pigment epithelium and Müller glia) and our in vivo RD, RD-PVR, and NMDA models will be performed. Retinal fibrosis will be evaluated with SD-OCT and histology. Aim 3: Evaluate the effects on intraocular pressure (IOP) and the ocular pharmacokinetics of clinically relevant MIF inhibitors. Rabbits will be used to determine the effects of the drugs on IOP and the pharmacokinetics of ocular delivery of MIF inhibitors.

2. KEYWORDS:

Retinal detachment (RD), proliferative vitreoretinopathy (PVR), N-methyl-D-aspartate (NMDA), macrophage migration inhibitory factor (MIF), MIF inhibitor, chick, rabbit, retinal pigment epithelium (RPE), ARPE-19, ibudilast, AV411, CPSI-1306, AV1013, gel contraction assay, TUNEL assay, epithelial mesenchymal transition (EMT)

3. ACCOMPLISHMENTS:

What were the major goals of the project?

Task 1. Evaluate the clinically relevant MIF inhibitors, CPSI-1306, ibudilast/AV1013 in our in vivo retinal damage models (RD and NMDA) for neuroprotection of photoreceptors.

This task will utilize electrophysiology, SD-OCT, fundus imaging, and TUNEL/IHC to assess the ability of MIF inhibitors to protect the retinal neurons in RD- and NMDA-induced retinal damage in chicks and find the appropriate dosage. This will include dose escalation studies in untreated animals with a single intravitreal injection in chicks to find a toxic and maximal therapeutic dose (1a). Dose ranging studies will be conducted in retinal damage models to find the optimal dose for neuroprotection (1b). Finally, drug timing studies will be performed to test the impact of timing on the neuroprotective benefit (1c).

Timeframe: Months 1-18

Subtask 1a. Perform dose escalation studies in untreated animals to find toxic and maximal therapeutic doses. This task will involve weighing, ocular examination with Nussenblat scale grading, IOP measurements, ERG, SD-OCT, and fundus imaging. This will be carried out on untreated chick eyes on a limited number of chicks (n=4).

Timeframe: Months 1-6

Y3Q1 Progress: None.

Y3Q2 Progress: None.

Y3Q3 Progress: None.

Y3Q4 Progress: None.

Remaining Tasks: None.

Completion: 27 chicks (27/27) + 18 ERG Tests (18/18) + 19 OCT Tests (19/19) + 22 normative ERG dataset chick measurements (22/22) + 12 normative OCT dataset chick measurements (12/12) + 13 TUNEL stains/analysis (13/13) + 12 DAPI INL thickness measurements (12/12) + Training & Protocol Generation (ERG,
OCT, Injection, Intubation, Slit Lamp, Fundus Imaging) (14) + Equipment (Tonopen, OCT Datastation, Fundus Camera, Injector, Isoflurane, Brooders x4, Intubation Tubes) (10) = 147 pts: 147/147 = 100%

Subtask 1b. Perform dose ranging studies for MIF inhibitors in retinal damage models. This task will be performed on a limited number of chicks (n=4) that have undergone retinal damage (RD or NMDA). They will be treated to find the optimal dose for neuroprotection with the MIF inhibitors. TUNEL analysis will be carried out on day 3 for RDs and day 1 for NMDA damaged retina. Following this study a larger study (n=10) will be carried out on day 14 (RD) or day 7 (NMDA) chicks with IHC, SD-OCT, fundus imaging, and ERG.
Timeframe: Months 1-18

Y3Q1 Progress: We conducted dose testing in the NMDA model at day 13 and the RD model at day 3 with ibudilast at 10-3 mg/mL and CPSI-1306 at 1.0 mg/mL. ERG and OCT were performed on NMDA treated chicks at day 1 and day 13. Data is pending.

Y3Q2 Progress: Pending data analysis was completed.

Y3Q3 Progress: Pending ERG data analysis was completed. Additional D1 and D14 RD experiments and D10 NMDA experiments were completed with 1.0 mg/mL CPSI-1306. Data is pending for these recent experiments.

Y3Q4 Progress: To improve rigor and address variability in NMDA datasets, we developed a new protocol for TUNEL analysis. TUNEL data outliers from previous experiments were re-stained, and new images were re-analyzed to improve accuracy. Specifically, the TUNEL analysis process was modified to focus on the damaged area only (INL), and a minimum threshold of TUNEL+ cells/mm^2 was set. Subjects with eyes below this threshold were excluded from analysis. The changes to the process are discussed in more detail in the "Changes in Approach" section. In addition, additional dose testing was performed for day 3 RD + ibudilast and day 14 RD + CPSI-1306. Data analysis from new experiments and re-analysis is ongoing.

Remaining Tasks: After completing remaining re-analysis, we will continue RD dose testing with longer day 14 timepoints. Additional animals will be added to previous experiments as needed for statistical significance.

Completion: ~402 chicks (402/402) + 54 ERG Test Subjects (32/54) + 101 OCT Tests (80/101) + 370 TUNEL stains/analysis (297/370) + 94 DAPI INL thickness measurements (43/94) + 34 NMDA Normative chicks (34/34) + Training & Protocol Generation (ERG, OCT, Injection, Intubation, Slit Lamp, Fundus Imaging) (14) + Equipment (Tonopen, OCT Datastation, Fundus Camera, Injector, Isoflurane, Brooders x4, Intubation Tubes) (10) = 1079: 912/1079 = 84.5%

Subtask 1c. Drug timing studies in retinal damage models to test the impact of timing on the neuroprotective benefit of MIF inhibitors.
RD and NMDA damage models will be treated with optimized MIF inhibitor dose 2-6 hours after damage initiation. TUNEL staining and retinal thickness measurements will be taken to evaluate the impact of MIF inhibitors on retinal neuroprotection following injury.
Timeframe: Months 4-18

Y3Q1 Progress: No significant progress. Data is pending.

Y3Q2 Progress: No significant progress. Data is pending.

Y3Q3 Progress: No significant progress.

Y3Q4 Progress: No significant progress.

Remaining Tasks: Additional experiments are needed to evaluate higher doses of each drug and to add additional animals for statistical power.

Completion: ~90 chicks (36/90) + 70 TUNEL stains/analysis (12/70) + 20 DAPI INL thickness measurements (0/20) + Training & Protocol Generation (Injection, Slit Lamp, Fundus Imaging) (3) + Equipment (Tonopen, Injector, Isoflo, Brooders x4) (7) = 94: 58/190 = 30.5%

Task 2. Evaluate the ability of clinically relevant MIF inhibitors, CPSI-1306 and ibudilast/AV1013 to block gliosis and pathological wound healing and to protect against PVR in traumatic RD. *In vitro* studies with ARPE19 (retinal pigment epithelium) and MIO-M1 (Müller glia) cell lines and *in vivo* RD & NMDA models will be used to assess MIF inhibitor's anti-gliotic and anti-fibrotic activity.
Timeframe: Months 3-36

Subtask 2a. Test the hypothesis that MIF inhibitors block gliosis and pathological wound healing responses *in vitro*. Human RPE (ARPE-19) and Müller glia (MIO-M1) cell lines will be incubated with TGFβ to mimic PVR conditions. The effect of clinically relevant MIF inhibitors will be tested through scratch assays to assess migration, MTT assays to assess proliferation, contraction assays, and epithelial mesenchymal transition (EMT) assays to assess which aspects of pathological wound healing may be impacted by the MIF inhibitor treatment. Additionally, the Ibudilast/AV1013 combination will allow for elucidation to the role phosphodiesterase in wound healing.
Timeframe: Months 6-30

Y3Q1 Progress: We tested the effects of different concentrations of MIF inhibitors on gel contraction of ARPE-19 cells. Using a Cell Biolabs CytoSelect 24-well Cell Contraction Assay kit and following the manufacturer's protocol, we measured the contraction over a period of 24 hours. Ibudilast, AV1013, and CPSI-1306 were all tested for their ability to influence contraction.

Y3Q2 Progress: Gel contraction assays were completed with two doses of CPSI-1306 over a 24 hour period to confirm previous findings. CPSI-1306 inhibition of ARPE-19 contraction was comparable to that of other MIF inhibitors.

Y3Q3 Progress: No significant progress. Transwell experiments are planned and we are awaiting delivery of necessary supplies.

Y3Q4 Progress: Transwell migration experiments were performed with TGFβ with or without serum added to the lower chamber as the chemoattractant. MIF inhibitors ibudilast and AV1013 were added to both chambers to test their effect on cell migration.

Remaining Tasks: Additional replicates of the transwell experiment are needed for statistical power.

Completion: Cell line Verification (2/2) + 1 cell line * With & Without TGFβ (2) * 4 tests * 3 drugs (not including vehicle) = 26: 25/26 = 96.1%

Subtask 2b. Test the hypothesis that MIF inhibitors block gliosis and pathological wound healing responses *in vivo*. Doses of MIF inhibitors shown to block TUNEL staining will be used to evaluate the effect on retinal gliosis in our RD and NMDA damage models. Retinas will be evaluated with immunostaining for GFAP to detect gliosis, aquaporin 4 to detect Müller glia and astrocyte changes, CD45 to detect microglia accumulation, and PCNA to evaluate cell proliferation of Müller progenitor cells at day 14 (RD) and day 7/10 (NMDA). Studies will be carried out in an *in vivo* rabbit PVR model to determine if intravitreal drug administration blocks PVR formation. Retinas will be graded with the Fastenburg grading scale.
Timeframe: Months 12-36

Y3Q1 Progress: No significant progress.

Y3Q2 Progress: We have found that the optimal working concentration for our GFAP antibody is 1:1000. Optimization of CD45 and AQP4 is underway.

Y3Q3 Progress: We are in the process of further optimizing CD45 and AQP4 immunofluorescence.

Y3Q4 Progress: Staining of tissues from several ibudilast and CPSI-1306 experiments in both NMDA and RD models is underway for GFAP, AQP4, CD45, and PCNA. We have found that PCNA and CD45 signals fade quickly, so only newer tissue is being stained for these markers.

Remaining Tasks: Complete remaining stains for GFAP, CD45, PCNA, and AQP4. Fluorescence analysis for each marker needs to be completed. Additional experiments may be needed to obtain fresh tissue for additional n to ensure adequate numbers with acceptable tissue quality for analysis.

Completion: ~70 chicks (67/70) + 350 stains (GFAP, AQP4, CD45, PCNA) (33/350) + ~70 Rabbits (0/70) + Working Concentrations Found (4/4) + Western Blot Validation (0/4) = 498: 104/498 = 20.9%

Task 3. Determine the ocular pharmacokinetics of clinically relevant MIF inhibitors and their effects on IOP in rabbits. In vivo studies in untreated chicks will be performed in parallel to Aim 1 to evaluate retinal drug levels after a single injection. The MIF inhibitor that shows the greatest promise in Aims 1/2 will be further evaluated in rabbits for pharmacokinetic properties. An assay will be developed by the Pharmacoanalytical Core Facility at OSU to analyze the plasma, vitreous, and retinal drug levels. ERG and SD-OCT will be used to assess potential retinal toxicity. Systemic organ toxicity will be evaluated through necropsy by the Veterinary Core facility.
Timeframe: Months 1-36

Task 3a. Pharmacokinetic study – A screening pilot study using chick, performed in parallel to Aim 1, will be performed to evaluate drug levels in the retina. One untreated chick will be treated with one (or two) intravitreal drug injections at multiple doses and retinal drug levels will be evaluated after 1 day using the assay developed by the Pharmacoanalytical Core facility.
Timeframe: Months 1-6

Y3Q1 Progress: No significant progress

Y3Q2 Progress: No significant progress

Y3Q3 Progress: No significant progress.

Y3Q4 Progress: Vitreous and retina were isolated from untreated chicks for PK assay development.

Remaining Tasks: Experimental groups have not yet been started.

Completion: ~18 chicks (18) + Assay Generation (4) + Equipment (Tonopen, Injector, Isoflurane, Brooders x4) (7) = 29: 7/29 = 24.1%

Task 3b. Pharmacokinetic study – An extended pilot study using chick, performed in parallel to Aim 1, will be performed to evaluate retinal drug levels after one (or two) intravitreal treatments of MIF inhibitors in untreated animals using an extended pilot study.
Untreated chicks (n=3) will be treated with one (or two) drug injections at 1-2 doses. Retinal and vitreous drug levels will be evaluated at day 1 and day 3.
Timeframe: Months 3-12

Y3Q1 Progress: No significant progress

Y3Q2 Progress: No significant progress

Y3Q3 Progress: No significant progress.

Y3Q4 Progress: Vitreous and retina were isolated from untreated chicks for PK assay development.

Remaining Tasks: Experimental groups have not yet been started.

Completion: ~36 chicks (36) + Assay Generation (4) + Equipment (Tonopen, Injector, Isoflurane, Brooders x4) (7) = 47: 7/47 = 14.9%

Task 3c. Rabbit pharmacokinetic study – The MIF inhibitor drug showing the most promise in Aims 1/2 will be further evaluated in rabbits for pharmacokinetic properties.
Untreated rabbit eyes (n=3) will be intravitreally injected with the MIF inhibitor dosing scheme established in Aim 1. Fellow eyes will remain untreated. Clinical examination and IOP measurements will be performed prior to harvest for drug level evaluation. The plasma, vitreous, and retinal drug levels will be analyzed at different timepoints with assays developed by the Pharmacoanalytical Core facility at OSU. ERG, SD-OCT, and fundus imaging will be used to assess potential retinal toxicity. Systemic organ toxicity will be evaluated by necropsy at the 168 hour timepoint by the Veterinary Core facility.
Timeframe: Months 24-36

Y3Q1 Progress: No significant progress

Y3Q2 Progress: No significant progress

Y3Q3 Progress: Rabbit retina, vitreous, whole blood, plasma, and platelet rich plasma were isolated from cadaver rabbit eyes obtained from ULAR. These samples will be used to test the pharmacokinetic assay in development.

Y3Q4 Progress: The PK assay is in development. We are coordinating with ULAR to train lab members on rabbit handling and techniques, as well as to obtain rabbit plasma from cadavers to use in assay development. We recently received two female New Zealand white rabbits to refine handling, imaging, and other experimental procedures.

Remaining Tasks: Experimental groups have not yet been started.

Completion: ~45 Rabbits (45) + ~15 ERG Tests (15) + ~15 OCT Tests (15) + Training & Protocol Generation (Rabbit ERG, Rabbit OCT, Rabbit Injection, Rabbit Slit Lamp, Rabbit Fundus Imaging) (10) + Equipment (Tonopen, OCT Datastation, Fundus Camera, Injector, Isoflo) (5) = 90: 5/90 = 5.6%

What was accomplished under these goals?

A. Subtask 1B

a. **Continued dose testing for ibudilast and CPSI-1306:** Dose testing continued in chicks for ibudilast and CPSI-1306 in both the RD and NMDA models. Doses of each drug that were most promising in the NMDA model were used to begin dose testing in RDs. To improve rigor and address variability in NMDA datasets, we developed a new protocol for TUNEL analysis (see details in “Changes in Approach” section). We are in the process of reanalyzing some previous data. Some results from this re-analysis are shown (**Fig 1**). These two graphs show the TUNEL ratios (A: with outliers, B: without outliers) from the reanalyzed data for ibudilast treatment at 0.00001 mg/ml, 0.001 mg/ml, 0.1 mg/ml and 1.0 mg/ml. Statistics were run through nonparametric multiple comparison testing with the Steel-Dwass method using JMP software. Comparing the TUNEL ratio for each drug dose we find a statistically significant dose-dependent decrease in TUNEL positive cells with ibudilast (ibudilast at 0.00001 mg/ml, $p = 0.3277$, ibudilast 0.001 mg/ml $p = 0.0117$ ($p = 0.0005$ without outliers, as determined per protocol), ibudilast 0.1 mg/ml $p = 0.0006$, and ibudilast 1.0 mg/ml $p = 0.0044$ ($p = 0.0002$ without outliers)). Not shown are data for CPSI-1306 and AV1013 at 1.0 mg/ml, neither of these

drugs/doses were significantly different from the control/control ratio with a paired analysis (CPSI-1306, p = 0.4898; AV1013, p = 0.2555). While some data remains to be reprocessed with other doses and conditions, the current results of this re-analysis validate our pursuit of ibudilast as a potential neuroprotective agent.

b. **Normative and NMDA damaged chick testing:** The publication in PLOS One highlights the testing of undamaged or normative chicks and NMDA damaged chicks with a variety of clinically relevant measurement techniques. This included IOP, Weight, OCT, and ERG. Briefly, we found that NMDA caused a trend towards lower intraocular pressures (**Fig 2A**) and that weight was unchanged between undamaged and NMDA damaged subjects (**Fig 2B**). Retinal thicknesses captured with optical coherence tomography showed the formation of edema immediately after NMDA damage with subsequent thinning in retinal layers. Interestingly, we also observed the formation for the first time of a hyperreflective band in the inner nuclear layer (**Fig 3**). Finally, measurements with electroretinograms showed the greatest functional loss immediately following the damage with some limited recovery in most metrics over time. While the ON-bipolar cells in our study were subject to the most lasting damage, the OFF-bipolar cells were reduced immediately after damage and recovered to near control amplitudes at later timepoints.(**Fig 4**). These studies set the stage to next evaluate the impact of MIF inhibitors on preservation of retinal function.

B. Subtask 2A

a. **Gel contraction assay**: We tested the effects of MIF inhibitors on gel contraction of ARPE-19 cells as our *in vitro* PVR model. Using a Cell Biolabs CytoSelect 24-well Cell Contraction Assay kit and following the manufacturer's protocol, we measured the contraction over a period of 24 hours. Ibudilast, AV1013, and CPSI-1306 were all tested for their ability to influence contraction. The contraction ratio was calculated by measuring the area of the gel at 24 hours and dividing it by the initial area at time 0. The ratios are calculated as a percent of control. MIF inhibitors were tested at different concentrations for their ability to inhibit ARPE-19 gel contraction. Inhibition of contraction indicates potential to inhibit a mechanism of retinal scarring that occurs in the critical condition of PVR. Our findings indicate that MIF inhibitors are able to inhibit contraction in a dose dependent manner (**Fig 5**).

b. **Transwell migration assay**: Cell migration is an essential step in PVR scar formation. This is why we tested the ability of MIF inhibitors to influence ARPE-19 cell migration in our *in vitro* PVR model. Transwell assay was used and TGFβ with or without serum was added to the lower chamber as the chemoattractant. The number of cells migrating from the upper to the lower chamber was quantified using a colorimetric assay. Our preliminary results indicate that ibudilast was able to inhibit ARPE-19 migration (**Fig 6**). Additional replicates are needed to confirm the findings, to test CPSI-1306 and AV1013, and to evaluate statistical significance.

C. Subtask 2B

a. **Antibody optimization:** Antibodies recommended by Dr. Fischer were titrated using our standard immunohistochemistry SOP at three different concentrations to determine the optimal amount of antibody for best quality imaging. PCNA required modification of our protocol to achieve sufficient signal. For this, the permeabilizing agent used was switched from Triton X to methanol. AQP4, PCNA, GFAP, and CD45 were optimized at 1:1000, the working concentration that will be used for all staining in this subtask.

b. **Immunohistochemical marker staining:** We have begun immunohistochemical marker staining to evaluate levels of gliosis, inflammation, and proliferation in several of our experimental conditions. Markers PCNA and CD45 have required some troubleshooting, as we discovered sectioned tissue that is 6 months or older loses the signal for these markers. GFAP and AQP4 have strong signals in older tissue. To ensure the best quality staining, tissue is stained as soon as possible after sectioning, and staining is done for PCNA and CD45 first to ensure full signal strength. Staining is partially completed for several experimental conditions (**Fig 7**).

D. Subtask 3A/3B

a. **Chick baseline samples for PK assay development:** Vitreous and retina from 28-day old untreated chicks were taken as baseline samples. These will be used to confirm efficacy of the PK assay in development by the OSU Pharmacoanalytic Shared Resource for future testing of chick samples. Dr. Cebulla met with Dr. Phelps at the Pharmacoanalytic Shared Resource to work on development of the PK assay and discuss study design, which will be relevant to IND application.

E. Subtask 3C

a. **Rabbit cadaver samples for PK assay development:** We obtained blood and cadaver eyes from two New Zealand white rabbits obtained through ULAR. Vitreous and retina were isolated. Whole blood, plasma, and platelet rich plasma were obtained for the various assays and rabbit PVR model. A protocol was optimized for the isolation of plasma and platelet rich plasma to standardize the process for upcoming rabbit experiments. Dr. Cebulla met with Dr. Phelps at the Pharmacoanalytic Shared Resource to work on development of the PK assay and discuss study design, which will be relevant to IND application.

b. **Rabbit training and protocol consultation with ULAR:** ULAR veterinarians are consulting with us on the protocol and assisting with planning safety aspects of the rabbit experiments. They have optimized processes to make procedures and imaging safer and more efficient. They have provided training to lab members on rabbit handling, blood draws, and USDA-required documentation, and will continue to support the project.

F. Publications, Manuscripts, and Presentations

a. The chick normative database paper “Multimodal imaging and functional analysis of chick NMDA retinal damage model” was published in PLOS One on September 7, 2021.
b. Manuscripts are in progress for our *in vitro* PVR work and impact on inflammatory, gliotic, and proliferative markers after damage.
c. Tyler Heisler-Taylor presented at the OSU Ophthalmology Graduate Research Day 2021 about the work from the PLOS One publication, winning 1st place among his peers for his presentation.
d. Tyler Heisler-Taylor presented at the Ohio Lions Eye Research Foundation annual meeting 2021 including some of the work from the PLOS One publication.
e. Richard Wan presented his Master’s thesis “Effect of MIF inhibitors Using a N-Methyl-D-Aspartate Damaged Chick Retina Model.” in June 2021.
f. Richard Wan won the “3 Minute Thesis” award, placing first at the College of Optometry as well as the University level of all graduate students for his presentation on the “Effect of MIF inhibitors Using a N-Methyl-D-Aspartate Damaged Chick Retina Model” in February 2021.
g. Dr. Cebulla presented data in an initial consultation with the Drug and Device Development Services Core at Nationwide Children’s Hospital (NCH) on 5/28/21. This group with the Office of Research Regulatory Affairs at NCH has extensive experience in helping investigators develop regulatory strategies to move toward clinical trials. They are reviewing the preclinical data and will work with Dr. Cebulla to develop a plan to apply for an IND if positive results are found.

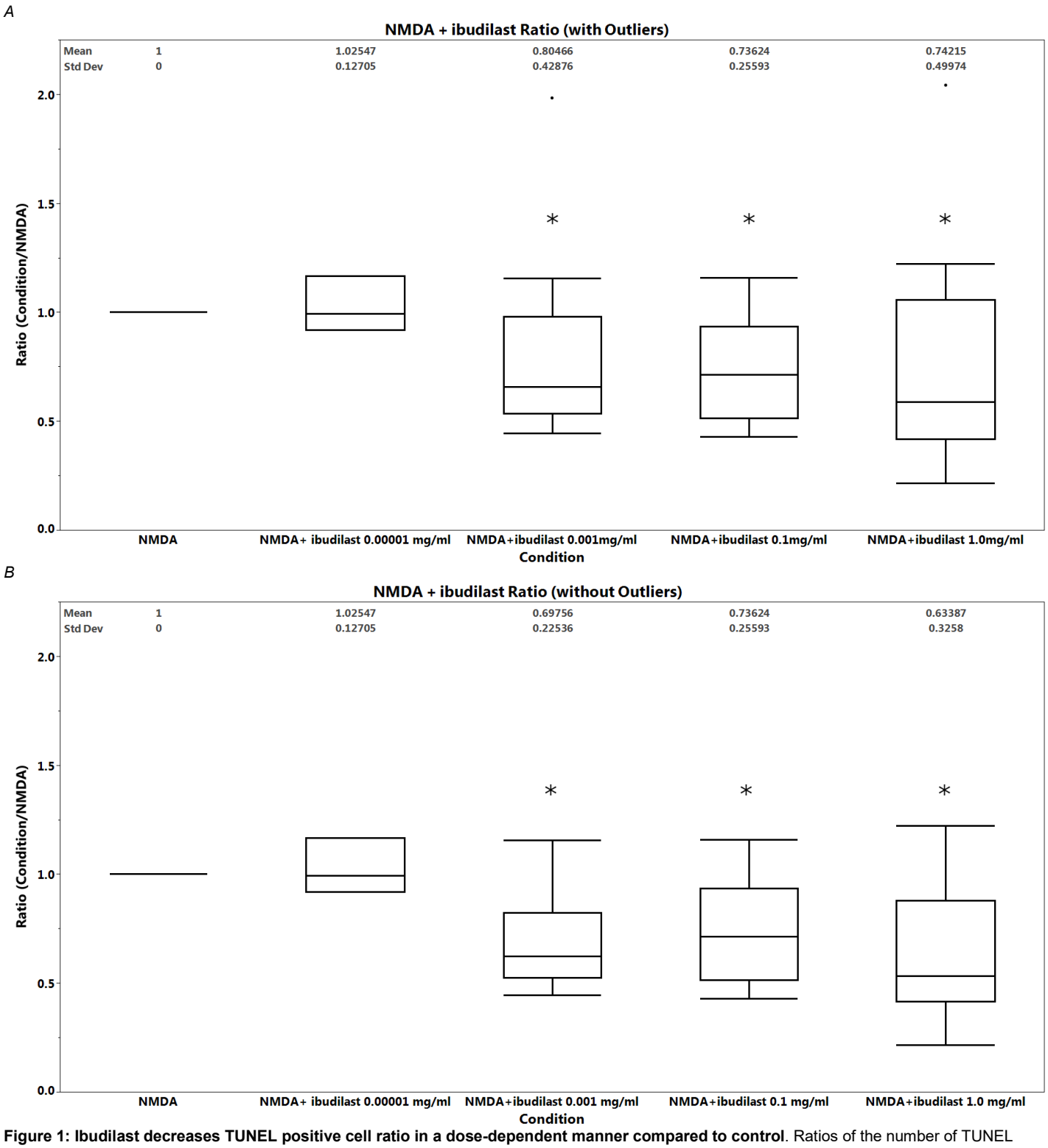

Figure 1: Ibudilast decreases TUNEL positive cell ratio in a dose-dependent manner compared to control. Ratios of the number of TUNEL positive cells in the INL in MIF inhibitor-treated compared to fellow-eye vehicle-treated NMDA damaged eyes are shown both with statistical outliers (A) and without (B). Statistical significance was evaluated with nonparametric multiple comparison testing correction with the Steel-Dwass method. Comparing each drug dose with the NMDA control ratio we find ibudilast at 0.00001 mg/ml is not significantly different from the control ratio (p = 0.3277 (n=3)), ibudilast 0.001 mg/ml is significantly lower (p = 0.0117 (n=12), (p = 0.0005 without outliers, n=11)), ibudilast 0.1 mg/ml is significantly lower (p = 0.0006 (n=6)), and 1.0 mg/ml is significantly lower (p = 0.0044 (n=13), (p = 0.0002 without outliers, n=12)). Mean and standard deviation are shown along the top of each graph. * indicate statistical significance.

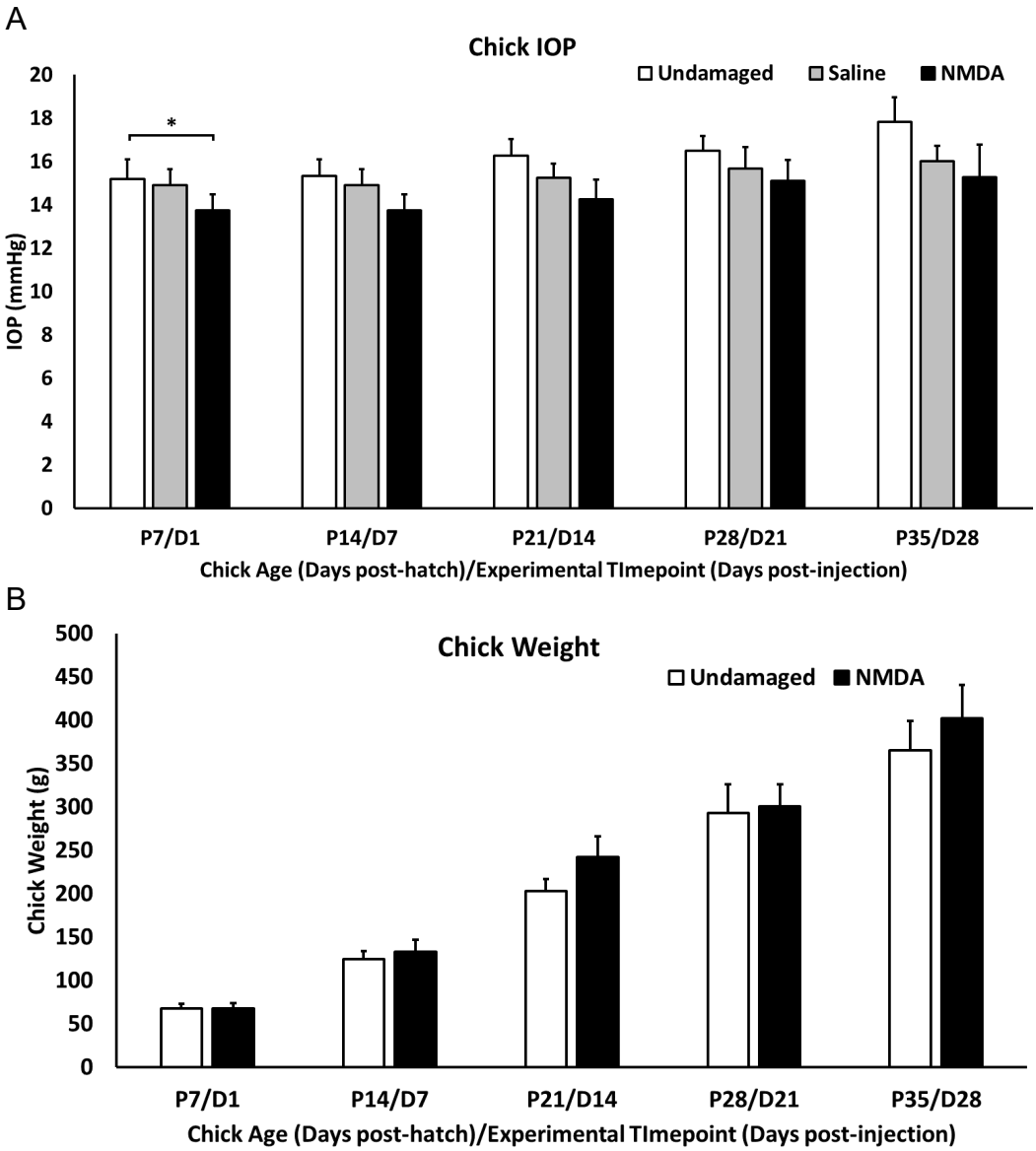

Fig 2. IOP & Weight measurements. A) Chick IOP measurements on undamaged chicks and NMDA-damaged chicks (OD: Saline, OS: NMDA) taken weekly starting at post-hatch day 7 (P7) / post-injection day 1 (D1) until P37/D28. There were no significant differences in IOP after day 1. **B)** A normative database of undamaged and NMDA-damaged chicks were weighed weekly up until P35. The two treatment groups were typically weighed within one day of each other except for the P21/D14 timepoint where the NMDA-damaged chicks were measured three days after the undamaged chicks due to experimental constraints (n=10/group).

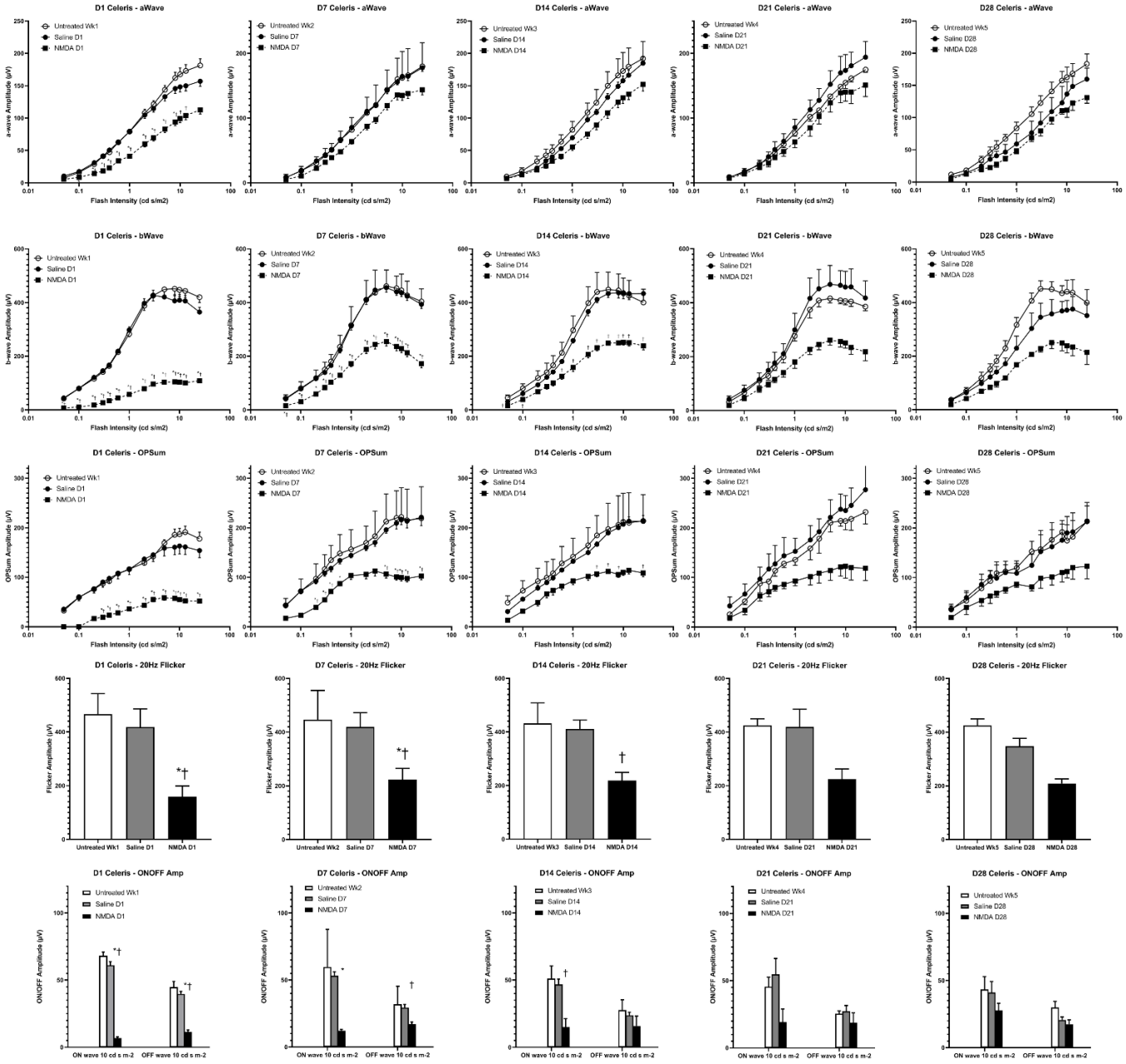

Fig 4. ERG results of NMDA-damaged, vehicle-treated, and age-matched undamaged controls. Undamaged chicks (n = 10 P7 to P21, n = 5 P28 to P35), NMDA-damaged chick eyes (OS), and saline vehicle-injected fellow chick eyes (OD) (n = 10, P7/D1 to P14/D7, n = 8, P21/D14, n = 6, P28/D21, n = 5, P35/D28) were examined with the Celeris ERG system. The data is organized by time (columns) and parameter (rows). From left to right, the columns represent one day post-injection (D1) and 7 days post-hatch (P7), D7/P14, D14/P21, D21/P28, and D28/P35. From top to bottom, the rows represent a-wave amplitudes, b-wave amplitudes, the amplitudes of the sum of oscillatory potentials (OPSum), flicker amplitudes at 20Hz, and ON/OFF bipolar cell response amplitudes. * indicates significance with vehicle (saline) controls, † indicates significance with undamaged controls.

.

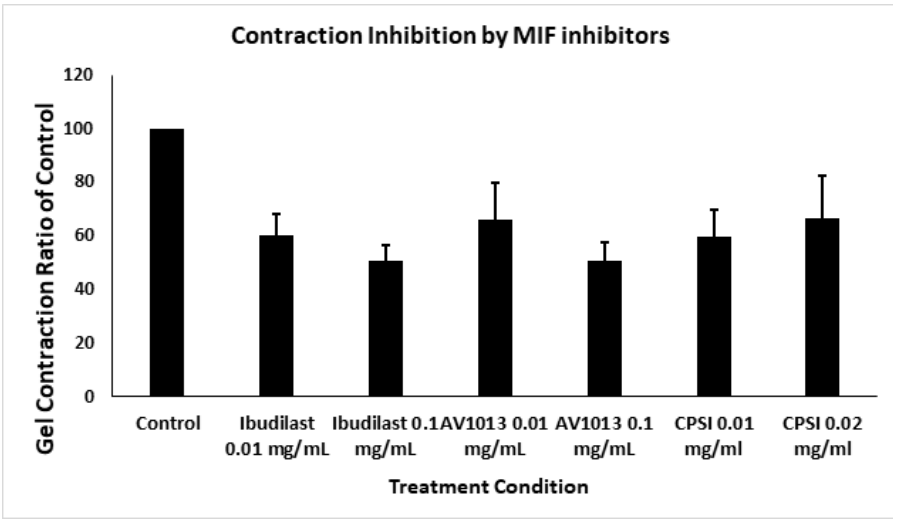

Figure 5. MIF inhibitors block collagen gel contraction in *in vitro* PVR model. ARPE-19 cells were treated with the indicated concentrations of MIF inhibitors while subjected to gel contraction studies in the *in vitro* PVR model. Results are shown as percent of control contraction (maximum gel contraction set at 100%). The contraction ratio was calculated by measuring the area of the gel at 24 hours and dividing it by the initial area at time 0.

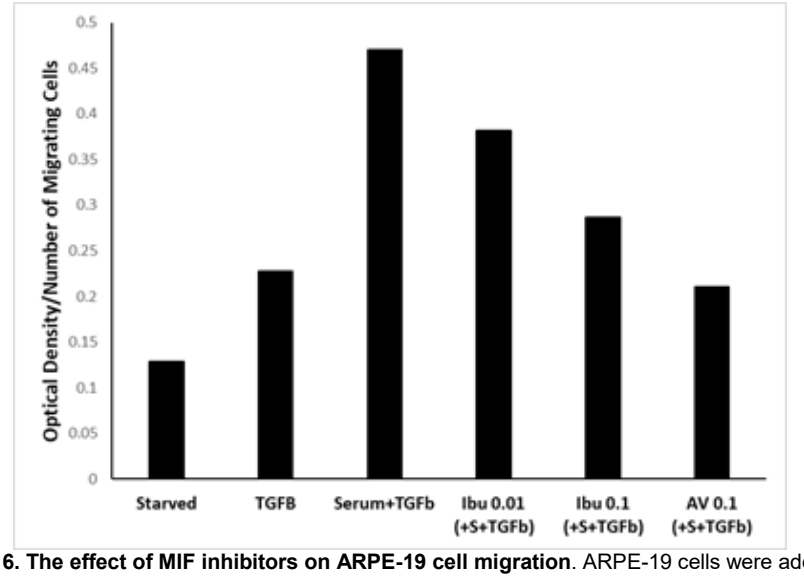

Figure 6. The effect of MIF inhibitors on ARPE-19 cell migration. ARPE-19 cells were added to the upper chamber of 24-well cell migration transwell assay plate. TGFβ with or without serum was added to the lower chamber. The indicated MIF inhibitor treatment was added to both chambers. After 24 hours, non-migrating cells were removed. Cells that migrated to the lower chamber were stained, extracted, and quantified using a plate reader. The experiment will be repeated and statistical analysis will be performed.

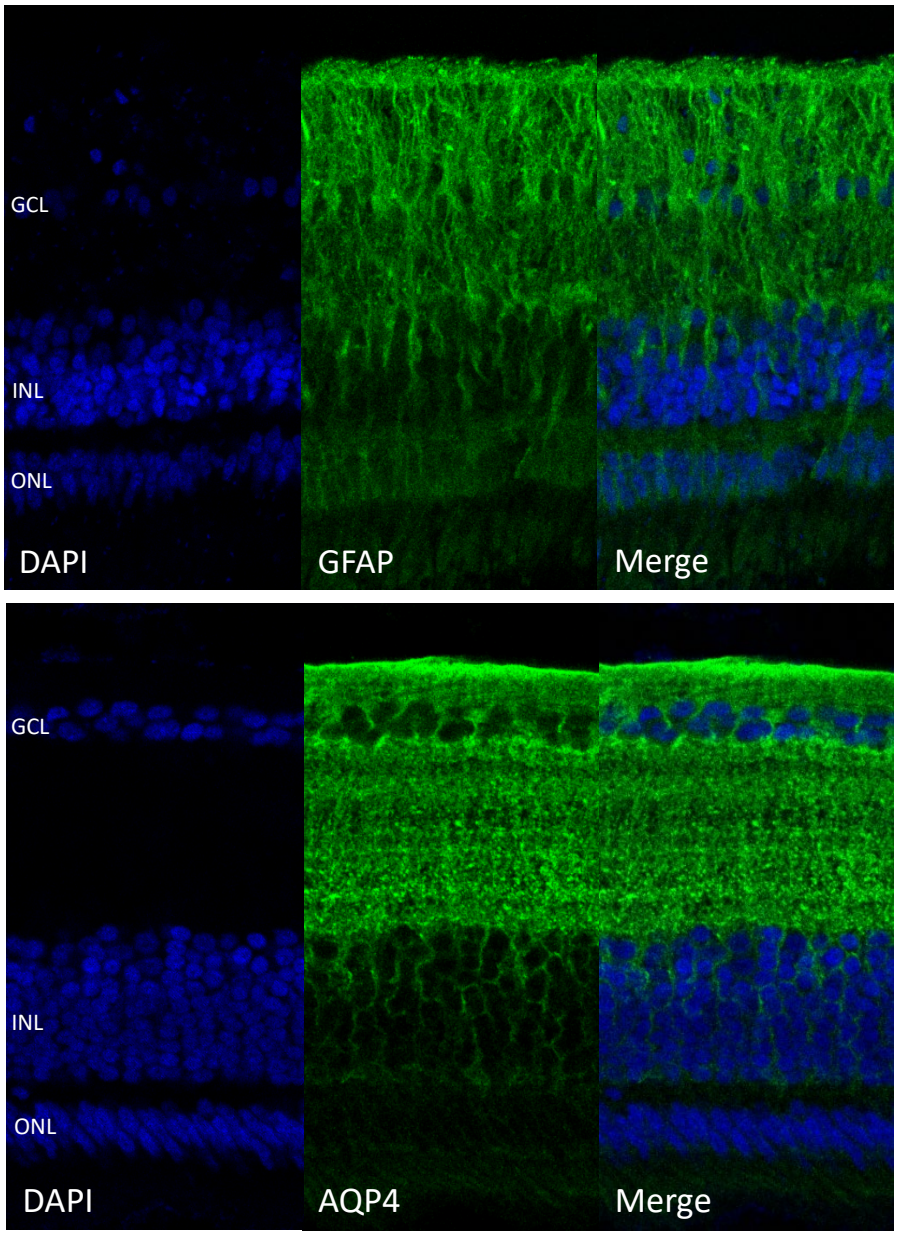

Figure 7. Sample images from immunohistochemistry optimization. Markers were titrated to optimal working concentrations. Staining for each marker has begun on several different experimental conditions. Each staining pattern was compared to references from literature. Example images are shown for GFAP (top) and AQP4 (bottom). PCNA and CD45 are not shown.

Professional Development Activities:
Manuscript covering the impact of MIF inhibitors from *in vitro* PVR experiments and the impact on gliosis, inflammation, proliferation *in vivo* are in preparation.

How were the results disseminated to communities of interest?

Normative ERG data in the chick is available to other vision investigators through the normative database manuscript published in PLOS One.

Presentations of data were delivered in the Department of Ophthalmology and Visual Sciences, the Ohio Lions Eye Research Foundation annual meeting, and the "3 Minute Thesis" competition at The Ohio State University. A presentation was given to the Drug and Device Development Services team at Nationwide Children's Hospital.

What do you plan to do during the next reporting period to accomplish the goals?
We are currently in the process of hiring a full time research assistant to help finish the project. Additional personnel may be hired if needed to complete the work on time. In the next period we plan to continue consulting and training with ULAR to perform the rabbit work. We will also continue to collaborate with Dr. Racine for methodology, analysis, and interpretation of rabbit ERGs. Finally, plans are in place to finish dose testing in the chick RD and NMDA models, and to begin the pilot PK studies in chicks.

4. IMPACT:

What was the impact on the development of the principal discipline(s) of the project?

The chick is an excellent model for vision research and the studies performed herein will expand the utility of the model for other vision scientists. The normative database studies on retinal structure and function (particularly with spectral domain optical coherence tomography (SD-OCT) imaging and electrophysiology studies) in normal and damage responses will expand knowledge of the chick eye as it relates to ophthalmic research. By understanding long-term effects of retinal detachment and excitotoxic damage on the chick eye, researchers will be able to extrapolate data from chicks used in research to gain further insight into what happens in the human eye under the same conditions. Chick and human eyes have two important similarities – a cone-driven retina, and the presence of a central high-density photoreceptor region (macula and area centralis), the point in the retina where visual acuity is highest. Having these features makes the chick eye an especially good model for the human eye, and a favorable alternative to mouse models of eye diseases. Mice dominate animal research for their well-understood genetics, and the ease and diversity of genetic manipulation available. However, mice also lack a macula and have a rod-driven retina as well as very low visual acuity. These differences from the human eye make mice a less-than-ideal model for studying ocular diseases and retinal pathologies. Continued study of normative measurements will allow for further understanding of the chick model of retinal damage. Further development and understanding of the chick retinal damage model may lead to its increased use in ophthalmic research as a fitting model for the human eye.

What was the impact on other disciplines?

Nothing to Report.

What was the impact on technology transfer?

Nothing to Report.

What was the impact on society beyond science and technology?

Nothing to Report.

5. CHANGES/PROBLEMS:

Changes in approach and reasons for change

To improve rigor and address variability in NMDA datasets, we developed a new protocol for TUNEL analysis to address these issues and are in the process of re-analyzing previous data. The re-analysis standardizes our data to minimize inter-subject variability and normalizes data to counter high biologic variability. This was performed by switching from measuring the total number of TUNEL positive cells per mm^2 of total retina (from the outer nuclear layer (ONL) to the ganglion cell layer (GCL)) to measuring the total number of TUNEL positive

cells per mm^2 of the inner nuclear layer (INL), which is the retinal layer damaged by NMDA. This is a similar measurement to our published work in the mouse RD model, where TUNEL positive cells were measured per mm^2 of the outer nuclear layer (ONL).
Furthermore, data was normalized by taking the ratio of the experimental treatment eye (left eye, OS, NMDA+MIF inhibitor) over the fellow control eye (right eye, OD, NMDA+vehicle). This ratio was calculated per retinal section, with n=3-4 paired retinal sections, obtained at different sectioning levels, from the same subject per slide. This analysis allowed us to introduce an exclusion criterion for subjects that had a high level of inconsistencies between the TUNEL ratios of the different retinal sections from the same individual. Subjects were excluded when inconsistencies in the ratio of experimental to control reached a coefficient of variation (CV) of ≥ 50% or standard deviation ≥ 0.5 between multiple sections from the same subject. For example, a subject was excluded when one pair of retinal sections had a 50% reduction in TUNEL positive cells per mm^2 with drug treatment, but another pair of sections on the same slide had a 150% increase in TUNEL positive cells per mm^2 with drug treatment.

Another established exclusion criterion was removing any subjects that produced control (NMDA+vehicle) TUNEL positive cell densities below a threshold of 1500 TUNEL+ cells/mm^2.

A final exclusion criterion was imposed: subjects whose average treatment over control ratio was identified as an outlier through the outlier analysis tools in JMP statistical software. Specifically, data was run through the Robust Fit Outliers tool and analyzed with Huber Outliers Test, Cauchy Outliers Test, and the Quartile Outliers test. Subjects that were identified as an outlier in at least one of the tests were flagged as outliers and excluded. Data are currently presented showing graphs and statistics with and without identified outliers.

The excluded subjects are flagged. Excluded subjects and reasons for exclusion are recorded in a separate tab in the analysis spreadsheet.

We will note that, as before, the TUNEL analysis is performed under masked conditions.

While some data remains to be re-processed, the current results of this re-analysis validate our pursuit of ibudilast as a potential agent for an IND application, with a dose-dependent reduction in TUNEL positive cells in the INL.

Actual or anticipated problems or delays and actions or plans to resolve them

To complete the project in a more timely manner, another full time lab member is required. We are in the process of hiring an additional full time research assistant to aid with the project.

It will be necessary for us to obtain additional installs of ERG Espion analysis software and Bioptigen SD-OCT Softwares (Diver and InVivo Vue) and Datastation computer so we can increase the speed of our analysis of the retinal imaging. Currently our single datastation and limited software installs creates a bottleneck and backlog of data, allowing only one user to analyze data at a time. We would like have multiple personnel working on the analysis to address this issue. This purchase will be necessary in order to finish the project during the period of the no cost extension. There is adequate budget for the purchase. The major cost is the software; the cost of the datastation computer is <$5000. The scope of work will not change.

Changes that had a significant impact on expenditures

Price changes related to animals drove up our spending. The price of one male chick increased from $1.44 to $2.21, and ULAR's per diem rates for brooder care increased slightly. We have also used more chicks than we initially planned and will continue to order them regularly until all necessary data is captured. We have obtained our first rabbits and their prices have significantly increased, approximately 2-fold, from the original budget. There are sufficient funds available to cover these increases.
The price estimates to conduct the pharmacokinetic studies to support IND level work with the OSU Pharmacoanalytic Shared Resource have also increased, but there are sufficient funds available to cover these increases.

Personnel has also affected expenditures. No post-doc was paid on the grant from 9/30/20 to 8/2/21, and we have now hired Sumaya Hamadmad as a post-doc. Our original subcontract with electrophysiologist Dr. Racine ended after year two, but she is needed to complete the ERG work for the no cost extension and her subcontract is being renewed with remaining funds.

Significant changes in use or care of human subjects, vertebrate animals, biohazards, and/or select agents

Significant changes in use or care of human subjects

Nothing to Report.

Significant changes in use or care of vertebrate animals

Nothing to Report.

Significant changes in use of biohazards and/or select agents

Nothing to Report.

6. PRODUCTS:

- **Publications, conference papers, and presentations**

  Journal publications.

  Heisler-Taylor T, Wan R, Urbanski EG, Hamadmad S, Shah MH, Wilson H, Racine J, Cebulla CM. PLoS One. 2021 Sep 7;16(9):e0257148. doi: 10.1371/journal.pone.0257148. eCollection 2021. PMID: 34492087

  Books or other non-periodical, one-time publications.

  Nothing to Report.

  Other publications, conference papers and presentations.

  Heisler-Taylor, Tyler; Wan, Richard; Urbanski, Elizabeth; Hamadmad, Sumaya; Shah, Mohd; Wilson, Hailey; Racine, Julie; Cebulla, Colleen. Multimodal imaging and functional analysis of the chick NMDA retinal damage model. OSU Ophthalmology Research Day 2021. 1st Place.

  Wan, Richard. Effect of MIF inhibitors Using a N-Methyl-D-Aspartate Damaged Chick Retina Model. Master's Thesis. The Ohio State University. 2021

- **Website(s) or other Internet site(s)**

  Nothing to Report.

- **Technologies or techniques**

  Nothing to Report.

- **Inventions, patent applications, and/or licenses**

  Nothing to Report.

- **Other Products**

  Nothing to Report.

7. PARTICIPANTS & OTHER COLLABORATING ORGANIZATIONS

What individuals have worked on the project?

Name: Dr. Colleen M Cebulla
No change.

Name: Dr. Andy J Fischer
Project Role: Co-investigator
Researcher Identifier (e.g. ORCID ID):
Nearest person month worked: 1
Contribution to Project: Recommended new CD45 antibody, provided troubleshooting and feedback on updated immunostaining protocol, provided troubleshooting for PCNA staining.

Name: Dr. Abhay Satoskar
No change.

Name: Dr. Julie Racine
Project Role: Co-investigator
Researcher Identifier (e.g. ORCID ID):
Nearest person month worked: 1
Contribution to Project: Consulted on chick ERG data analysis, generated new ERG protocols for rabbit ERGs, and recommended new electrodes for rabbit ERG.

Name: Dr. Mitch Phelps
Project Role: Co-investigator
Researcher Identifier (e.g. ORCID ID):
Nearest person month worked: <1
Contribution to Project: Consulted on development of pharmacokinetic study design and assay development to support IND application if positive results are found.

Name: Dr. Kevin Bosse
Project Role: Consultant
Researcher Identifier (e.g. ORCID ID):
Nearest person month worked: <1
Contribution to Project: Consulted for regulatory support for IND application.

Name: Tyler Heisler-Taylor
No change.
Funding Support: Ohio Lions Eye Research Foundation Norbert Peiker Eye Research Fellowship

Name: Elizabeth Urbanski
No change.

Name: Richard Wan
No change.

Name: Sumaya Hamadmad

No change.

Name: Hailey Wilson
No change.

Name: Mohamed Soumakieh
No change.

Name: Yushin Jeng
Project Role: Student Research Assistant
Researcher Identifier (e.g. ORCID ID):
Nearest person month worked: 2
Contribution to Project: Recorded clinical exam data during animal experiments, completed TUNEL staining and microscopy, performed literature review, assisted in training new undergraduate volunteers, embedded and sectioned frozen tissue, and provided lab organization.

Has there been a change in the active other support of the PD/PI(s) or senior/key personnel since the last reporting period?

Colleen M Cebulla

Status: Active
Title: Full Field OCT for Cellular Level Structural and Functional Retinal Imaging
Grant Number: R01EY031098
Sponsoring Organization: NEI/NIH
Role: Co-Investigator
Dates Active: 9/01/2020- 08/31/2024

Status: Active
Title: My Virtual Cancer
Grant Number: DE-SC0021630
Sponsoring Organization: DOE
Role: Co-Investigator/Site PI
Dates Active: 05/01/2021-11/01/2021

Status: Active
Title: Torsional Indirect Traumatic Neuropathy (TITON): Animal model for diagnostics, drug delivery, and therapeutics for central nervous system injury
Grant Number: W81XWH-15-1-0074 P00001
Sponsoring Organization: USAMRAA (DOD)
Role: Co-Investigator
Dates Active: 03/29/2019-03/28/2022

Status: Active
Title: Characterization of the role of MIF on retinal health and disease
Grant Number: 1R01EY032573
Sponsoring Organization: NEI/NIH
Role: PI
Dates Active: 09/01/2021 – 06/30/2026

Status: Active
Title: Germline genetic determinants of transformation of uveal nevi to melanoma: towards early diagnosis and prevention of disease progression
Grant Number: ME200199

Sponsoring Organization: USAMRAA (DOD)
Role: Co-Investigator
Dates Active: 09/30/2021-09/29/2024

Status: Active
Title: Ohio Lions Research Grant
Sponsoring Organization: Ohio Lions Eye Research Foundation
Role: PI
Dates Active: 06/01/2013-09/14/2022

Status: Pending
Title: The Ohio State University vision sciences research core program (OSU-VSRCP)
Grant Number: P30 TBD
Role: Co-I
Sponsoring Organization: NIH/NEI

Andrew J Fischer
Status: Active
Title: Fatty acid binding-proteins and endocannabinoids in the retina; roles in glial reactivity and reprogramming of Muller glia into progenitor cells
Grant Number: RO1 EY032141-01
Role: PI
Sponsoring Organization: NIH/NEI
Dates Active: 01/01/2021 – 01/31/2026

Status: Active
Title: Muller glia: roles in retinal homeostasis and neuronal regeneration
Grant Number: RO1 EY022030-09
Role: PI
Sponsoring Organization: NIH/NEI
Dates Active: 12/30/2019 – 06/30/2022

Status: Active
Title: Fatty acid binding-proteins and endocannabinoids in the retina; roles in glial reactivity and reprogramming of Muller glia into progenitor cells
Grant Number: RO1 EY022030-09 supplement
Role: PI
Sponsoring Organization: NIH/NEI
Dates Active: 09/01/2020 – 06/30/2022

Status: Active
Title: Development of neuronal subtypes and local circuits in the hippocampus
Grant Number: R01MH124870-01
Role: Co-I
Sponsoring Organization: NIH/ National Institute of Mental Health
Dates Active: 07/01/2021 – 04/30/2026

Status: Active
Title: Characterization of the role of MIF on retinal health and disease
Grant Number: RO1 EY032573-01
Role: Co-I
Sponsoring Organization: NIH/NEI
Dates Active: 09/01/2021 – 06/30/2026

Status: Active
Title: X chromosome inactivation in sex disparities to substance use disorder

Grant Number: DP1 DA054344
Role: Co-I
Sponsoring Organization: NIH/National Institute on Drug Abuse
Dates Active: 08/15/2021 – 05/30/2026

Status: Pending
Title: Muller glia: reprogramming and neural regeneration in the retina
Grant Number: RO1 EY022030-10
Role: PI
Sponsoring Organization: NIH/NEI
Dates Active: 06/30/2022 – 06/30/2027

Status: Pending
Title: The Ohio State University vision sciences research core program (OSU-VSRCP)
Grant Number: P30 TBD
Role: Co-I
Sponsoring Organization: NIH/NEI

Status: Pending
Title: Prenatal opioids and neonatal withdrawal, and their cellular and molecular consequences in the developing brain
Grant Number: R21 TBD
Role: Co-I
Sponsoring Organization: NIH/NEI

Status: Pending
Title: Impact of cannabis abuse on the function of astrocyte network
Grant Number: R21 TBD
Role: Co-I
Sponsoring Organization: NIH/NEI

What other organizations were involved as partners?

Nationwide Children's Hospital
Columbus, OH
Dr. Julie Racine, PhD continues to collaborate with and advise the lab on ERG experiments. She has also generated several protocols using Diagnosys software for our experiments, and most recently has helped us generate protocols and methodology for rabbit ERGs.

Nationwide Children's Hospital
Columbus, OH

Kevin Bosse, PhD, RAC, Director, Office of Research Regulatory Affairs, The Drug and Device Development Services Core at Nationwide Children's Hospital. This core has extensive experience in helping investigators develop regulatory strategies to move toward clinical trials. Dr. Bosse met with Dr. Cebulla and his team is reviewing her data and will work to help support an IND application if the study results are positive.

8. SPECIAL REPORTING REQUIREMENTS

COLLABORATIVE AWARDS: Nothing to Report.

QUAD CHARTS: See attached.

9. APPENDICES:
See attached.

PLOS ONE

RESEARCH ARTICLE

Multimodal imaging and functional analysis of the chick NMDA retinal damage model

Tyler Heisler-Taylor[1,2], Richard Wan[1,3], Elizabeth G. Urbanski[1], Sumaya Hamadmad[1], Mohd Hussain Shah[1], Hailey Wilson[1], Julie Racine[4], Colleen M. Cebulla[1]*

1 Department of Ophthalmology and Visual Sciences, Havener Eye Institute, The Ohio State University Wexner Medical Center, Columbus, Ohio, United States of America, **2** Department of Biomedical Engineering, The Ohio State University, Columbus, Ohio, United States of America, **3** College of Optometry, The Ohio State University, Columbus, Ohio, United States of America, **4** Nationwide Children's Hospital, Columbus, Ohio, United States of America

* colleen.cebulla@osumc.edu

OPEN ACCESS

Citation: Heisler-Taylor T, Wan R, Urbanski EG, Hamadmad S, Shah MH, Wilson H, et al. (2021) Multimodal imaging and functional analysis of the chick NMDA retinal damage model. PLoS ONE 16(9): e0257148. https://doi.org/10.1371/journal.pone.0257148

Editor: Alexandre Hiroaki Kihara, Universidade Federal do ABC, BRAZIL

Received: May 14, 2021

Accepted: August 24, 2021

Published: September 7, 2021

Peer Review History: PLOS recognizes the benefits of transparency in the peer review process; therefore, we enable the publication of all of the content of peer review and author responses alongside final, published articles. The editorial history of this article is available here: https://doi.org/10.1371/journal.pone.0257148

Data Availability Statement: All relevant data are within the manuscript and its Supporting information files.

Abstract

Objectives

The chick is rapidly becoming a standardized preclinical model in vision research to study mechanisms of ocular disease. We seek to comprehensively evaluate the N-methyl-D-aspartate (NMDA) model of excitotoxic retinal damage using multimodal imaging, functional, and histologic approaches in NMDA-damaged, vehicle-treated, and undamaged chicks.

Methods

Chicks were either left undamaged in both eyes or were injected with NMDA in the left eye and saline (vehicle) in the right eye. TUNEL assay was performed on chicks to assess levels of retinal cell death one day post-injection of NMDA or saline and on age-matched untreated chicks. Spectral domain optical coherence tomography (SD-OCT) was performed weekly on chicks and age-matched controls day 1 (D1) up to D28 post-injection. Light adapted electroretinograms (ERG) were performed alongside SD-OCT measurements on post-injection chicks along with age-matched untreated controls.

Results

Untreated and vehicle-treated eyes had no TUNEL positive cells while NMDA-treated eyes accumulated large numbers of TUNEL positive cells in the Inner Nuclear Layer (INL), but not other layers, at D1 post injection. Significant inner retina swelling or edema was found on SD-OCT imaging at D1 post-injection which resolved at subsequent timepoints. Both the INL and the inner plexiform layer significantly thinned by one-week post-injection and did not recover for the duration of the measurements. On ERG, NMDA-treated eyes had significantly reduced amplitudes of all parameters at D1 with all metrics improving over time. The b-wave, oscillatory potentials, and ON/OFF bipolar responses were the most affected with at least 70% reduction immediately after damage compared to the fellow eye control.

Funding: The U.S. Army Medical Research Acquisition Activity, 820 Chandler Street, Fort Detrick MD 21702-5014 is the awarding and administering acquisition office. This work was supported by the Department of Defense, through the Vision Research Program under Award No. W81XWH1810805. Opinions, interpretations, conclusions and recommendations are those of the author and are not necessarily endorsed by the Department of Defense. In conducting research using animals, the investigators adhere to the laws of the United States and regulations of the Department of Agriculture. The authors acknowledge funding support from the Ohio Lions Eye Research Foundation (OLERF) and the Norbert Peiker Ohio Lions Eye Research Foundation Fellowship.

Competing interests: The authors have declared that no competing interests exist.

Conclusion

This study establishes a normative baseline on the retinal health and gross functional ability as well as intraocular pressures of undamaged, vehicle-treated, and NMDA-damaged chicks to provide a standard for comparing therapeutic treatment studies in this important animal model.

Introduction

Animal models are critical to understand the mechanisms of retinal disease and potential treatments. A damage model that has been commonly used in chicks and other species is the NMDA (N-methyl-D-aspartate) excitotoxic damage model [1–3], which mimics glutamate excitotoxic damage in the retina. Glutamate excitotoxicity occurs when a surplus of glutamate, a neurotransmitter, forms in the retina due to either excessive release or inadequate clearance by glutamine synthetase [4–6]. This excess glutamate activates NMDA receptors on inner retinal neurons which function as Ca^{2+} pumps into the cells. The resulting increase in intracellular Ca^{2+} acts as a second messenger and triggers a cascade that leads to eventual cell death [7–12]. This cell death can occur through both apoptotic and necrotic pathways depending on the glutamate or NMDA concentration [7]. This damage can be seen in diseases like glaucoma, retinal ischemia, vascular occlusion, diabetic retinopathy, sickle cell retinopathy, retinopathy of prematurity, and blast injury [7,13–16]. The NMDA retinal damage model simulates glutamate excitotoxicity by injecting NMDA into the vitreous cavity, which will activate the NMDA receptor, and cause Ca^{2+} induced cell death [14].

In contemporary vision research, the domestic White Leghorn chick (*gallus gallus domesticus*) has become increasingly popular in serving as an ocular model that offers translational parallels to the human eye. The chick has several advantageous features and may currently be underutilized for ocular research [13]. Because the chick is an avian species that utilizes diurnal color vision [17,18], its eyes have a cone-rich retina [19–21] and a high-density region of photoreceptors called the area centralis [22–24], anatomically translatable to human's cone-rich retina and macula. The chick eye is much larger than the mouse eye, making it a more preferred model when administering intraocular injections. Chicks are also more cost efficient for high throughput testing [13].

Despite strides in the understanding of retinal cellular signaling during damage, there have been no multimodal studies comparing functional and structural changes in NMDA-damaged eyes vs controls. We seek to establish a baseline of biometric data in healthy and NMDA-damaged chicks, including key technology like the electroretinogram (ERG) to analyze the electrical function of retinal cells and spectral domain optical coherence tomography (SD-OCT) to view the retinal layers in live subjects. In our NMDA chick model, the greatest damage has been shown to be primarily localized to the inner nuclear layer (INL) [1]. We will also analyze intraocular pressure (IOP), weight, and cell death through the TUNEL assay so that future researchers may have a benchmark for future studies testing druggable targets to ameliorate excitotoxic damage.

Materials and methods

Animals

The use of animals in these experiments was in accordance with guidelines established by the National Institutes of Health and the principles of the ARVO Statement for Use of Animals in Ophthalmic and Vision Research. It was conducted under a protocol approved by The Ohio

State University Institutional Animal Care and Use Committee. Newly hatched wild type leghorn chickens (*gallus gallus domesticus*) were obtained from Meyer Hatchery (Polk, Ohio). Postnatal chicks were housed in a stainless-steel brooder at around 32˚C and kept on a 12-hour light, dark cycle. Water and Purina™ chick starter were provided *ad libitum*. Chicks were weighed prior to any treatments or sacrifice timepoints. Slit lamp observations and fundus imaging with an operating microscope were taken prior to any measurements. These studies utilized 4 chicks for TUNEL analysis, 20 chicks for the initial round of ERG/OCT/etc testing, and 14 chicks for the supplemental ERG/OCT/etc testing making a total of 38 chicks.

Chick anesthesia

The chicks were kept warm to maintain an internal temperature of 40.3–40.8˚C via a heating pad and blanket (a double folded cut of surgical cloth) during surgical and clinical procedures and under a heat lamp at all other times.

The chicks underwent general anesthesia via a Kent Scientific VetFlo Calibrated Vaporizer. The anesthesia exposure duration was recorded to mitigate overexposure and potential harm to the animals.

Chick injection

5% betadine, an antiseptic topical solution, was prophylactically administered on the ocular surface of each eye, and then the superior eyelid and periocular region were swabbed with betadine solution via a cotton-tipped applicator. The betadine was left to dry for at least 30 seconds before inserting a 25μL Hamilton syringe or a 29Ga Insulin Syringe through the superior palpebra penetrating the globe into the posterior segment. 20μL of NMDA (25mM) was slowly injected intravitreally into the left eye (OS) and the syringe was slowly withdrawn from the globe approximately 5 seconds after the injection was complete [25,26]. The eye was then rinsed with sterile saline to wash out any residual betadine. The same procedure was performed on the fellow chick eye (right eye, OD) with sterile saline, the vehicle control. Chicks were injected and sacrificed at three timepoints. Chicks were injected at post-hatch day 7 (P7) and sacrificed one day after injection (D1) for cell death (TUNEL) analysis, sacrificed two weeks after injection (P21 or D14), and sacrificed 4 weeks after injection (P35 or D28).

Tonometry

The iCare Tonovet Plus was used to measure intraocular pressure on chicks before and after each injection and weekly before any other operations. Post-injection measurements were taken 3–10 minutes afterwards in order for the pressure to normalize. The iCare Tonovet Plus was used on the lapine or rabbit setting and was found to produce similar readings to those reported in the literature [27–31]. The iCare Tonovet Plus was operated according to the manufacturer's instructions with both eyes of each chick being measured consecutively over an average of five readings.

Spectral domain optical coherence tomography

SD-OCT was performed on chicks on both eyes weekly after the initial injection of NMDA using an Envisu R2200 SDOIS, a rabbit bore lens, and the InVivoVue software. Prior to beginning, chicks were anesthetized via isoflurane following the protocol previously stated. A chick was then placed on an imaging mount and the nose cone of the isoflurane line was secured at the rat bite bar to sustain controlled anesthesia throughout the process. To maintain a continual clear view, the chick eye was secured open with a small, lid speculum (2mm barraquer wire

eye speculum) and hydrated with Systane Ultra drops, as needed. The chick position was adjusted until the pectin, located inferiorly in the retina, was positioned in the central inferior view on the imaging program (S1 Fig).

On each eye, three scans were acquired: a 12mm 1000x1x60 frames (1000 A-scans per B-scan, 1 B-scan, 60 B-scans per frame) linear B-scan for high quality images, a 12x12mm 1000x6x25 frames radial scan for data collection, and a 12x12mm 400x400x4 frames volumetric scan for volume intensity projection (VIP) views. The captured scans were then averaged in InVivoView and analyzed in InVivoVue Diver. In the Diver software, 8 measurements points were selected (S1B Fig) approximately 1-2mm from the pecten allowing the measurements of various but consistent retinal thicknesses (S1C Fig).

Electroretinography

All ERGs were performed under the guidance of a trained visual electrophysiologist. Light adapted ERGs were first recorded with the use of the UTAS 3000 system (LCK Technologies Ltd.). Light adapted ERG were also recorded with the Celeris (Diagnosys, LLC) system on an independent set of chicks. For the duration of the testing, chicks were kept anesthetized (isoflurane; as mentioned above) with rectal temperature monitored and maintained between 40.3–40.8˚C.

For the UTAS system, a ground wire needle (Grass E2 subdermal electrode) was subcutaneously inserted under the wing and the reference electrode needle (Grass E2 subdermal electrode) at the posterior end of the head. A drop of 0.5% tetracaine was administered topically to provide corneal anesthesia. A DTL Plus Electrode (Diagnosys, LLC) was positioned on the chick such that the electrode fiber rested over the pupil of the eye. Genteal Severe Gel or Refresh Celluvisc was topically administered to keep cornea moist during testing. Each chick was laid on their side and the chick's eye was positioned centrally inside the ERG ganzfeld. Right eye was tested first followed by the left eye. However, with the Celeris system, no subdermal electrodes were required. Genteal Severe Gel was topically administered to the Celeris bright flash stimulators (5mm apparatuses) to facilitate electrical contact and keep the cornea moist. Stimulator were placed on each eye as per the manufacturer's recommendations and both eyes were tested in an alternating manner.

Light adapted electroretinograms were recorded every 7 days from post hatch day 7 to 35. Electroretinograms (bandwidth (UTAS): 0 to 500 Hz, bandwidth (Celeris): 0.125 to 300 Hz) and oscillatory potentials (bandwidth (UTAS): 75 to 500 Hz, bandwidth (Celeris): 75 to 300 Hz) were recorded simultaneously. The light adapted ERGs and OPs (background: 30 cd/m^2) were evoked to flashes of white light (flash duration less than 4 ms) spanning over a 2 log unit range with a minimal intensity of 0.062 (Celeris: 0.05) and maximal intensity of 25 cd.sec/m^2. Averages of 20 responses were taken at each step. An interstimulus interval (ISI) of 1 sec was used throughout the testing period.

Amplitude of the a-wave was measured from the baseline to the first negative trough while that of the b-wave was measured from the a-wave trough to the most positive peak of the ERG. The amplitude of all OPs was also summated to yield the OPSum value. Peak times were measured from the flash onset to the peak of each component. Light adapted flicker ERGs were also recorded. Background was set at 30 cd/m^2 with a flash intensity of 4.4 cd.sec/m^2 (Celeris: 5 cd.sec/m^2) and a frequency of 15, 20 and 25 Hz. Amplitude was measured from the preceding through to each positive peak. Long flash stimulation was also recorded. Background intensity was set at 30 cd/m^2 with flash intensity of 4.4 cd.sec/m^2 (Celeris: 5 and 10 cd.sec/m^2) with ISI of 5 seconds and a flash duration of 150 ms. Amplitude of the ON response a-wave was measured from the baseline to the first negative trough while that of the ON response b-

wave was measured from the a-wave trough to the most positive peak of the ERG. Amplitude of the OFF responses was measured from the flash offset to the most positive peak after the flash offset.

TUNEL

TUNEL assay was performed according to the manufacturer's instructions (TMR red kit, cat#: 12156792910, Roche) to detect cell death in the retina INL. The assay stained at 568nm (red) while a nuclear counterstain was applied with DAPI at 461nm (blue). Images were taken with a Leica DM5000B fluorescent microscope and Leica DC500 digital camera at 200x magnification with the Leica Application Suite 4.8.0 software. Exposure settings were adjusted to minimize oversaturation. Cells were counted utilizing the MCT method [32].

Statistical analysis

Data were analyzed in a masked fashion and calculated in Microsoft Excel and JMP. ERG data were processed and analyzed in Graphpad PRISM before entry into JMP for statistical analysis. The Kruskal-Wallis non-parametric test was performed to evaluate differences between experimental groups and the Steel-Dwass non-parametric post-hoc testing for multiple comparisons. Error bars are listed with standard error of the mean (SEM) unless stated otherwise and an $\alpha = 0.05$.

Results

Clinical observations

Slit lamp observations of the external ocular surface and anterior segment as well as fundus imaging of the posterior segment and retinal surface showed no media opacity on undamaged and vehicle eyes. Most eyes displayed some degree of punctate epithelial erosions, likely due to the process of repeated measurements. In NMDA-damaged eyes, while it was difficult to find the pecten, it was clear and sharp indicating a lack of media opacity, however the retina itself had changed from pink with visible scleral veins prior to any injections (Fig 1A) to a foggy white coloration (Fig 1B). NMDA damage was not found to impact chick weight gain (S2 Fig).

Intraocular pressure

IOP was measured before and after injections and weekly up until sacrifice on undamaged, vehicle (saline) injected, and NMDA-damaged eyes (n = 10/group D1-D14, n = 5/group D21-D28, Fig 2). While NMDA trended lower than controls at each of the timepoints, it was only significantly lower than undamaged eyes at the P7/D1 timepoint (Undamaged: 15.20 ±0.89mmHg vs. NMDA: 13.74±0.73mmHg, p = 0.0075). Additionally, there were significant increases over time as the chick aged in all three conditions (NMDA, vehicle, and undamaged). IOP variations were within the clinically acceptable range of only few mmHg in difference and could have been due to a multitude of factors including normal diurnal changes to the IOP, difference in researcher measurement technique, and tonometer variation. When comparing the IOP measurements of NMDA and vehicle (saline) treated eyes from pre- and post-injection measurements, we saw no significant differences whether immediately after the injection or a day later.

TUNEL

Select representative images were chosen to display the difference between untreated (n = 4), vehicle-treated (n = 4), and NMDA-treated TUNEL fluorescent captures (n = 4, Fig 3).

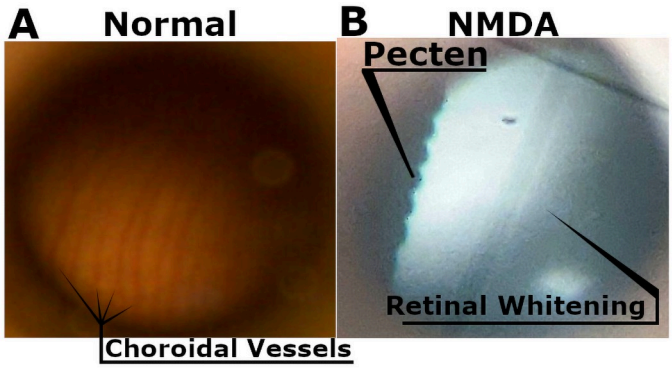

Fig 1. Representative fundus imaging. Choroidal vessels are visible in healthy chick eyes (A). While in NMDA-damaged chick eyes they can no longer be observed, instead we see the retina assume a homogenous white color potentially due to a lack of perfusion (B). The sharp and clear presence of the pecten rules out media opacity in NMDA-damaged eyes.

https://doi.org/10.1371/journal.pone.0257148.g001

Untreated and vehicle eyes were observed to contain no TUNEL positive cells indicating the lack of cells undergoing either apoptosis or necrosis. NMDA-damaged eyes however exhibited significant accumulation of TUNEL positive cells (3624.94 ± 449.51 vs. 0.00 ± 0.00 TUNEL positive cells/mm^2, p = 0.0211 vs untreated).

SD-OCT

Chicks treated with NMDA (OS) and vehicle (saline, OD) as well as age-matched undamaged controls were imaged with SD-OCT at D1, D7, D14, D21, and D28 with retinal thickness calculated from the resulting B-scans (Fig 4). Retinal thickness was calculated for the retinal nerve fiber layer (RNFL), inner plexiform layer (IPL), a combination of the RNFL and IPL,

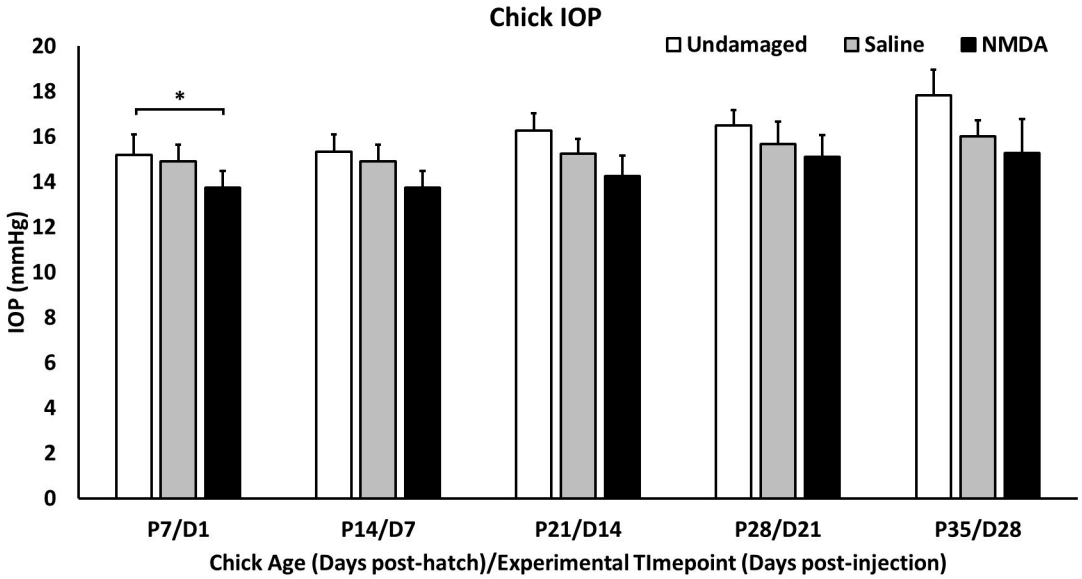

Fig 2. IOP measurements. Chick IOP measurements on undamaged chicks and NMDA-damaged chicks (OD: Saline, OS: NMDA) taken weekly starting at post-hatch day 7 or post-injection day 1 till post-hatch day 35 or post-injection day 28.

https://doi.org/10.1371/journal.pone.0257148.g002

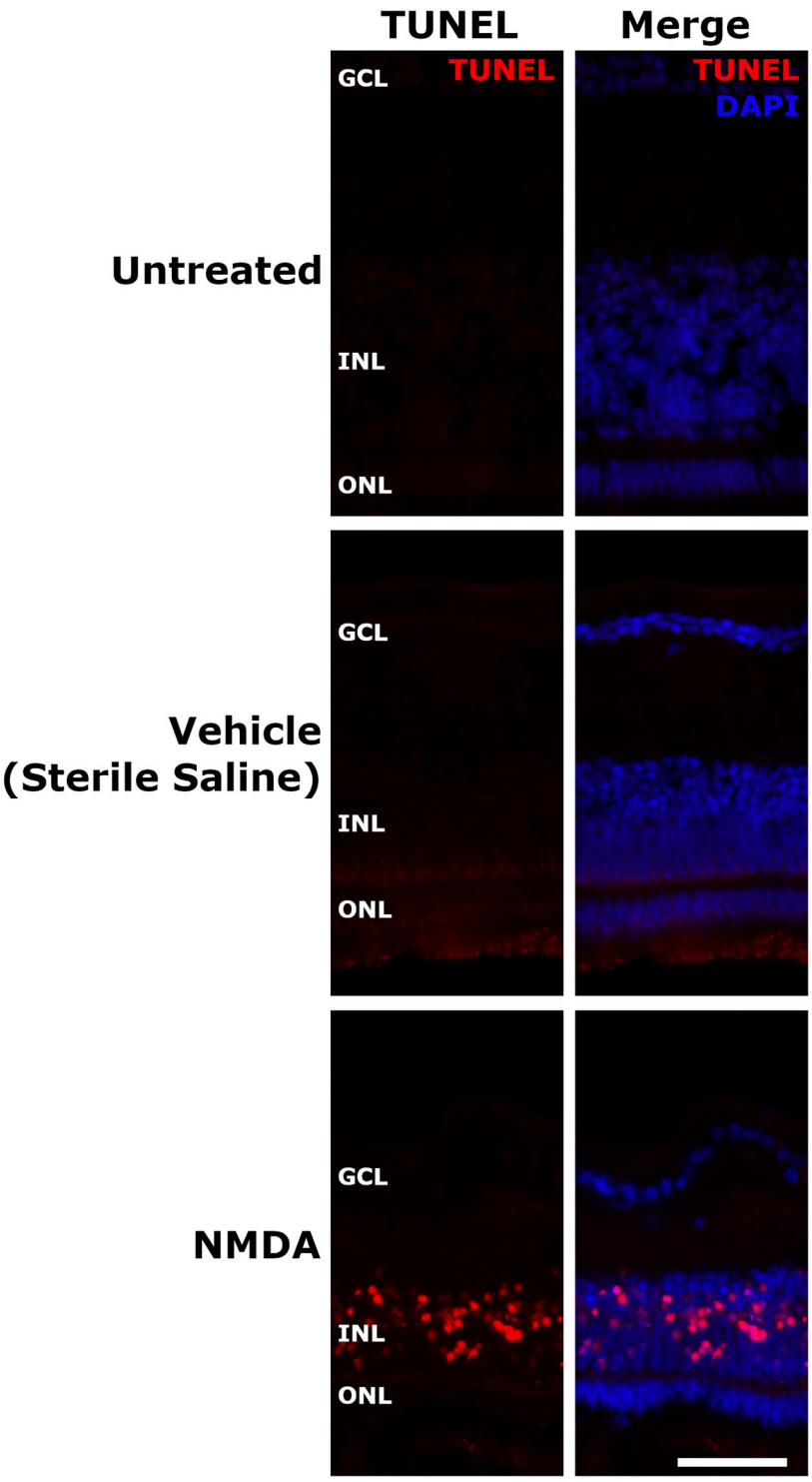

Fig 3. NMDA induced TUNEL response in chick retina. Untreated, vehicle (sterile saline), and NMDA injected chicks at D1 post injection. Both untreated and vehicle-injected chicks displayed no TUNEL-positive cells. NMDA-treated chicks saw a large number of TUNEL-positive cells in the INL, but not other retinal layers. The scale bar denotes 50μm. Abbreviation: GCL—ganglion cell layer, INL—inner nuclear layer, ONL—outer nuclear layer.

https://doi.org/10.1371/journal.pone.0257148.g003

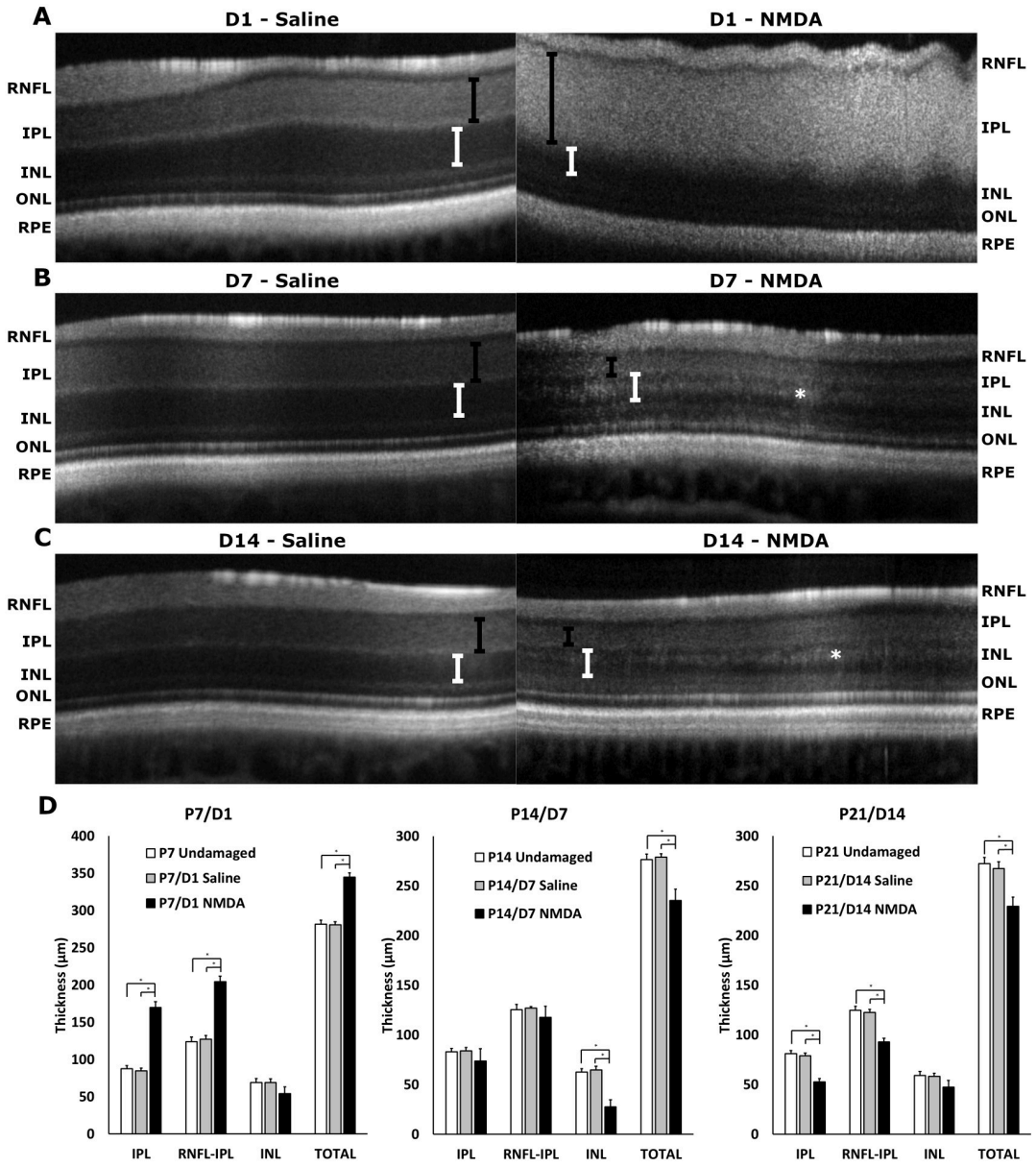

Fig 4. SD-OCT analysis of NMDA-treated and corresponding control eyes. Representative b-scans of D1 vehicle (saline, left) and D1 NMDA (right) showing edema in IPL (A), D7 vehicle (saline, left) and D7 NMDA (right) (B), and D14 vehicle (saline, left) and D14 NMDA (right) (C). (D) Analysis of retinal thicknesses of the IPL, RNFL-IPL combined, INL, and total thickness between NMDA and saline (vehicle) treated eyes at P7/D1 to P21/D14 post injection and their respective age-matched untreated controls. Black brackets show IPL thickness, white brackets show INL thickness, asterisk denotes hyperreflective layer. Error bars are shown as standard deviation. Abbreviations: RNFL—retinal nerve fiber layer, IPL—inner plexiform layer, INL—inner nuclear layer, ONL—outer nuclear layer, RPE—retinal pigment epithelium.

https://doi.org/10.1371/journal.pone.0257148.g004

INL, outer plexiform layer (OPL), outer nuclear layer (ONL), external limiting membrane (ELM), photoreceptors (PR), retinal pigment epithelium (RPE), and total thickness. Significant differences between NMDA-damaged eyes and controls were found in the IPL, INL, and total thickness (Fig 4D). Other layers were found to be unchanged (S2D Fig). Average thickness

values were used to compose a model to visually display the morphologic changes in the retina over time (Fig 6A).

The significant differences observed at D1 post-injection (Fig 4A) were most evident in the IPL with the presence of an inner retinal edema in the NMDA-treated eyes (Saline: $p = 0.0151$, Untreated: $p = 0.0151$, Fig 4D). Due to this edema, the RNFL-IPL combination and total retinal thicknesses of NMDA-treated eyes were significantly increased over controls. The INL appeared to begin thinning at D1 however the different was only borderline significant (Saline: $p = 0.0545$, Untreated: $p = 0.0545$, Fig 4D). One-week post-injection (D7) the retinal swelling had resolved and the effected layers became significantly thinner (Fig 4B). Most affected were the IPL becoming non-significant (Saline: $p = 0.5863$, Untreated: $p = 0.6977$, Fig 4D), the INL becoming significantly lower than controls (Saline: $p<0.0151$, Untreated: $p<0.0151$, Fig 4D), and the Total retinal thickness going from significantly higher to significantly lower than controls (Saline: $p<0.0151$, Untreated: $p<0.0151$, Fig 4D). The retinal thinning continued at D14 as the IPL and RNFL-IPL displayed the greatest reduction becoming significantly lower than controls (Saline: $p = 0.0151$, Untreated: $p = 0.0151$, Fig 4C). This thinning in the IPL counteracted the apparent reduction in thinning observed in the INL resulting in the total thickness remaining roughly the same as the previous timepoint, potentially a result of a new hyperreflective region within the INL (Fig 4B and 4C). The pattern observed at D14 continued during the subsequent timepoints at D21 and D28 (Fig 6A).

Electroretinogram

The a-wave serves as a metric for the function of cone photoreceptor and cone OFF-bipolar cells [33]. NMDA treatment was found to have the most significantly reduced a-wave amplitudes at D1 (38% reduction at 5cd.sec/m^2) with recovery at later timepoints (10% reduction at D28 at 5cd.sec/m^2) as NMDA appeared to recover towards controls (Fig 5 –top row and Fig 6B). The b-wave, which serves as a metric for the functionality of bipolar cells [33], was expected to show the most impairment in the NMDA damage model due to excitotoxic damage preferentially affecting bipolar and amacrine cells (Fig 5 –second row and Fig 6B) [25]. At D1, the NMDA-damaged eyes were significantly different from both controls at almost every flash intensity (75% reduction at 5cd.sec/m^2). From D7 through to D21, the damage profile remained similar with a 44% reduction at 5cd.sec/m^2 across these timepoints. By the final timepoint, the retinal function had restored up to a 30% reduction at 5cd.sec/m^2.

Oscillatory potentials, which summarizes the functionality of amacrine cells [33], were summed and compared similar to the a- and b-wave (Fig 5 –third row and Fig 6B). Akin to the b-wave, there was a large reduction of amplitudes at D1 (63% reduction at 5cd.sec/m^2) that did not show recovery like the a-wave (38% reduction at D28 at 5cd.sec/m^2). The flicker response, which encapsulates the function of the cone pathway [33], was not found to display significant differences between 15, 20, and 25Hz. The 20Hz data was chosen to show the differences between NMDA, vehicle, and undamaged eyes (Fig 5 –fourth row and Fig 6B). At most timepoints, NMDA was significantly lower than both controls (D1: 62% reduction, D28: 40% reduction).

The long flash ON/OFF response test allows separate measures for the functionality of the ON and OFF cone bipolar cells. The ON-bipolar response was found to show significant differences between NMDA damage and both controls from D1 (89% reduction) to D14 (68% reduction). At D28, the amplitude had recovered to only a 32% non-significant reduction. The OFF-bipolar response was only significant between NMDA and both controls at D1 (71% reduction) and D7 (42% reduction). By D28, the amplitude reduction had fallen to 15% (Fig 5 –bottom row and Fig 6B). This would indicate that ON bipolar cells are potentially more

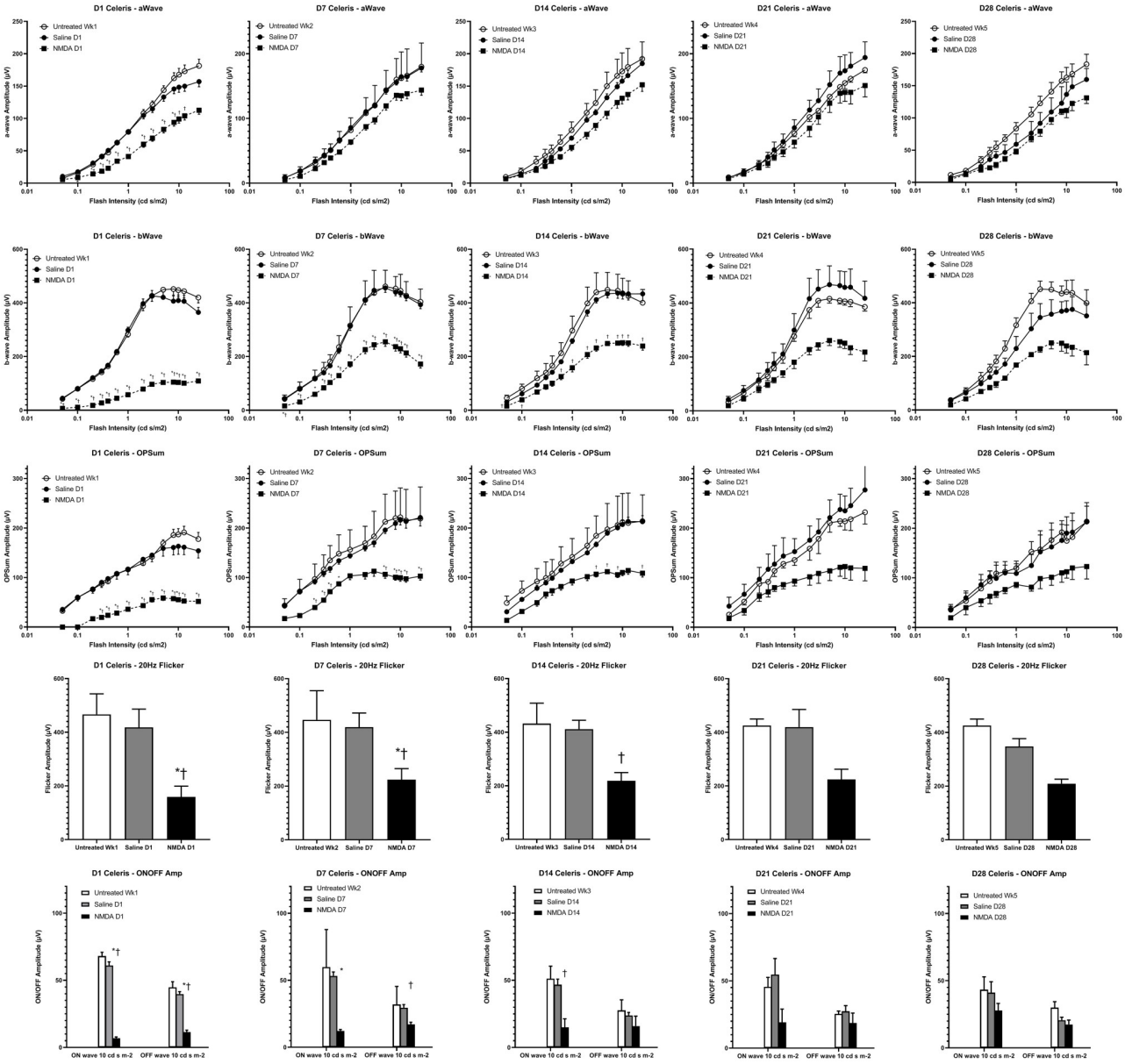

Fig 5. ERG results of NMDA-damaged, vehicle-treated, and age-matched undamaged controls. Undamaged chicks (n = 10 P7 to P21, n = 5 P28 to P35), NMDA-damaged chick eyes (OS), and saline vehicle-injected fellow chick eyes (OD) (n = 10, P7/D1 to P14/D7, n = 8, P21/D14, n = 6, P28/D21, n = 5, P35/D28) were examined with the Celeris ERG system. The data is organized by time (columns) and parameter (rows). From left to right, the columns represent one day post-injection (D1) and 7 days post-hatch (P7), D7/P14, D14/P21, D21/P28, and D28/P35. From top to bottom, the rows represent a-wave amplitudes, b-wave amplitudes, the amplitudes of the sum of oscillatory potentials (OPSum), flicker amplitudes at 20Hz, and ON/OFF bipolar cell response amplitudes. * indicates significance with vehicle (saline) controls, † indicates significance with undamaged controls.

https://doi.org/10.1371/journal.pone.0257148.g005

sensitive than OFF bipolar cells to NMDA damage. However, the reason behind this difference will be investigated in future studies.

Data captured with the Celeris ERG system (Fig 5) was found to be similar to data captured with the UTAS ERG system (S3 Fig). This is notable as both systems use fundamentally different designs to capture the ERG waveforms. While the Celeris system uses dual electrode

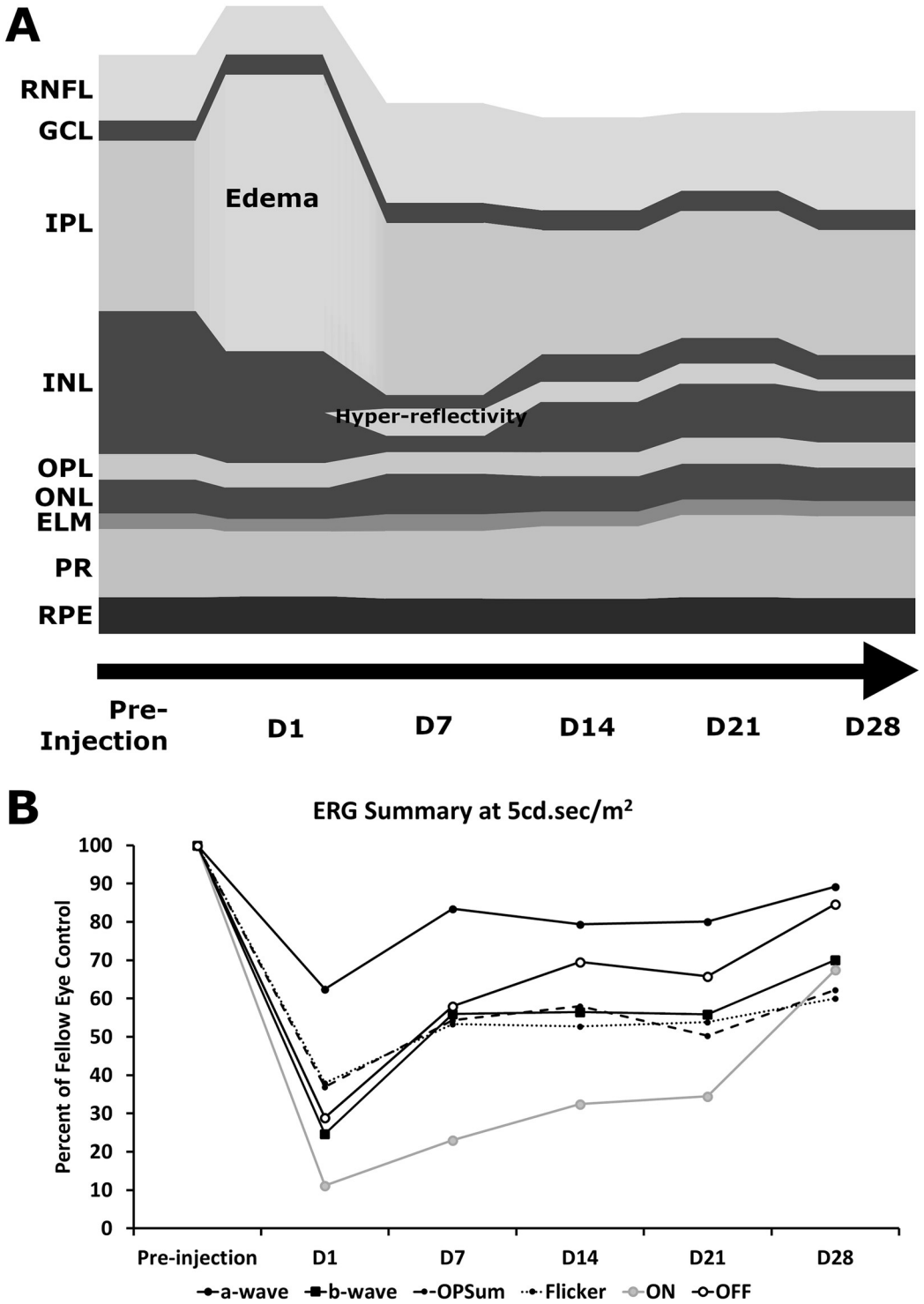

Fig 6. Quantitative characteristic model of SD-OCT and ERG behavior during chick NMDA damage. SD-OCT uses average layer thicknesses of NMDA-damaged chick eyes from D1 to D28 showing key features such as the edema present at D1 in the IPL and the hyperreflectivity present from D7 onwards in the INL (A). The ERG summary shows the average amplitudes as a percent of the fellow eye control at the 5 cd.sec/m^2 flash intensity from D1 to D28 (B).

https://doi.org/10.1371/journal.pone.0257148.g006

stimulators that come into close contact with the ocular surface, the UTAS system uses the more traditional ganzfeld approach.

Discussion

Despite the importance of the chick and the NMDA model for vision research, little normative data is available. This work is necessary to further develop the model to evaluate druggable targets for translational research. Herein we provide the first multimodal data on retinal structure and function in the chick NMDA model.

Interestingly we observed decreased ERG a-wave amplitudes at D1 despite a lack of TUNEL positive cells in the photoreceptor layers. Due to contributions of OFF-bipolar cells to the a-wave [33], this decrease in the a-wave amplitude could potentially be due to the disruption of the cone OFF-bipolar cells immediately after damage. While the ON-bipolar cells in our study were subject to the most lasting damage, the OFF-bipolar cells were only significantly reduced immediately after damage and recovered to near control amplitudes after D1. There is some contradictory data in the literature surrounding the effects of NMDA damage on the ON- and OFF- cone bipolar cells. One study of the effects of NMDA on rod and cone bipolar cells using a patch clamp technique found that NMDA significantly reduced response amplitudes of rod bipolar cells while the cone bipolar cells, both ON and OFF, were unaffected [34]. In contrast, another study observed almost complete ablation of both ON and OFF cone bipolar cells after combined NMDA and kainate damage [35]. Future studies may help resolve these discrepancies.

The most striking feature present in the SD-OCT imaging of the D1 NMDA retina was the retinal edema in the IPL. Following this initial swelling, the retina contracted considerably with the edema disappearing altogether, a behavior that has been noted in the established literature [25,36]. However, with this recovery and thinning of the IPL, the INL was observed to thicken slightly with the noted presence of a hyperreflective band on SD-OCT. As the edema on SD-OCT resolved at subsequent timepoints (Figs 4A and 6A), the a-wave amplitudes were noted to recover. Combining the edema resolution with the a-wave and OFF-bipolar cell recovery, we can hypothesize that the recovery of the edema is correlated with the a-wave and therefore OFF-bipolar cell recovery. Interestingly, the edema and hyperreflectivity in the inner retina with subsequent thinning is analogous to OCT scans of human retinal vascular occlusions [37–40].

In NMDA-damaged chick eyes, we observe significant levels of cell death in the INL consistent with the known loss of primarily amacrine cells in the inner retina [25,26,41,42]. Amacrine cells and the retinal ganglion cells (RGC) have been established as possessing NMDA-receptors, however in the chick model RGCs are rarely affected by NMDA damage [9,43–46]. While the other retinal neurons such as the photoreceptors, horizontal cells, and bipolar cells are generally considered to lack these receptors [9,47]. The loss of the amacrine cells, which are located in the INL and contribute to the oscillatory potentials [33], coincides with the large number of TUNEL positive cells in the INL and the amplitude reduction in the oscillatory potentials. In addition, we can see direct evidence of the retinal damage through the fundus imaging as the healthy pink color gives way to a retinal whitening, correlating with retinal edema and potentially further evidence of the ischemic conditions that lead to cell death. Despite lacking NMDA-receptors, bipolar cells are also strongly affected by NMDA damage through a potential TNFα glial cell pathway [48]. The b-wave amplitudes are not only severely diminished but the photopic hill effect is almost completely abrogated and remained muted even in subsequent timepoints. The photopic hill is a noted effect observed and heavily studied in human b-wave responses. It occurs due to the cone response of the bipolar cells with logistic

and gaussian curves [49–52]. Due to the diurnal nature of chicks, this effect can be directly observed (Fig 5—second row and Fig 6B) as the b-wave will reach a peak amplitude before starting to decline with further increases in flash intensity. This directly contrasts with the nocturnal models of mice and rats, which do not possess the cone density required for this effect.

While the chick model has many advantages for vision research, it does lack the breadth of genetic manipulation compared to more traditional mouse models. It is also unknown how repeated weekly anesthesia events could affect ocular parameters, particularly on the ERG. While efforts were taken to minimize diurnal changes, there remains the possibility that ERG results could shift in the hours between data acquisition. Additionally, due to electrode malfunctions, an additional batch of chicks had to be used to complete the D14/P21 and D21/P28 timepoints which could explain the discrepancies observed in ERG at those timepoints.

In conclusion, with this multimodal analysis of baseline chick ocular responses to NMDA excitotoxic damage, the stage is set for novel therapeutics to be tested. The chick eye proves to be more analogous to the human eye than other standard lab animal models between an area centralis, cone density, and the photopic hill effect. With the range of clinical disorders the chick NMDA model simulates including observable similarities to vascular occlusions, this could be a low-cost, simple model for high-throughput studies to develop and translate effective therapies to prevent vision loss.

Supporting information

S1 Fig. SD-OCT marker positions and fundus projection. (A) Representative capture of chick retinal layers with the pecten shown in the center. (B) Layer identifiers used by the InVivoView Diver software to measure retinal thicknesses. (C) Representative fundus capture from volumetric OCT scan. Blue crosses represent where measurements were taken. D) Measurements of all retinal thicknesses of the RNFL, IPL, RNFL-IPL, INL, OPL, ONL, ELM, PR, RPE, and full retina layers between NMDA and saline (vehicle) treated eyes at P7/D1 to P35/D28 post injection and their respective age-matched untreated controls. Error bars are shown as standard deviation. Abbreviations: RNFL—retinal nerve fiber layer, GCL—ganglion cell layer, IPL—inner plexiform layer, INL—inner nuclear layer, OPL—outer plexiform layer, ONL—outer nuclear layer, ELM—external limiting membrane, PR—photoreceptors, IS—inner segment, OS—outer segment, ETPRS—end tip of photoreceptors, RPE—retinal pigment epithelium.
(TIF)

S2 Fig. Weight measurements. A normative database of undamaged and NMDA-damaged chicks were weighed weekly up until sacrifice at P35. The two treatment groups were typically weighed within one day of each other except for the P21/D14 timepoint where the NMDA-damaged chicks were measured three days after the undamaged chicks due to experimental constraints (n = 10/group).
(TIF)

S3 Fig. In vivo ERG UTAS system measurements. Undamaged chicks (n = 3), NMDA-damaged chick eyes (OS), and saline vehicle-injected fellow chick eyes (OD) (n = 3) were examined with the In Vivo ERG UTAS System. The data is organized by time (columns) and parameter (rows). From left to right, the columns represent one day post-injection (D1) and 3 weeks post-hatch (PWk3), D6/PWk4, and D13/PWk5. From top to bottom, the rows represent a-wave amplitudes, b-wave amplitudes, the amplitudes of the sum of oscillatory potentials (OPSum), flicker amplitudes at 20Hz, and ON/OFF bipolar cell response amplitudes. *

indicates significance with vehicle (saline) controls, † indicates significance with undamaged controls.
(TIF)

S1 File.
(ZIP)

S2 File.
(ZIP)

Acknowledgments

The authors would like acknowledge the support of Dr. Andy J. Fischer, Isabella Palazzo, and Dr. Ralph Malbrue for their expertise with the chick model. The authors would like to thank Mahsa Adib, Haanya Ijaz, Yushin Jeng, and Mohamed Soumakieh for their technical assistance.

Author Contributions

Conceptualization: Tyler Heisler-Taylor, Julie Racine, Colleen M. Cebulla.

Data curation: Tyler Heisler-Taylor, Elizabeth G. Urbanski, Colleen M. Cebulla.

Formal analysis: Tyler Heisler-Taylor, Richard Wan, Hailey Wilson.

Investigation: Tyler Heisler-Taylor, Richard Wan, Elizabeth G. Urbanski, Sumaya Hamadmad, Mohd Hussain Shah, Hailey Wilson.

Methodology: Tyler Heisler-Taylor, Richard Wan, Elizabeth G. Urbanski, Sumaya Hamadmad, Julie Racine.

Project administration: Colleen M. Cebulla.

Resources: Julie Racine, Colleen M. Cebulla.

Software: Tyler Heisler-Taylor, Julie Racine.

Supervision: Julie Racine, Colleen M. Cebulla.

Validation: Tyler Heisler-Taylor.

Visualization: Tyler Heisler-Taylor.

Writing – original draft: Tyler Heisler-Taylor.

Writing – review & editing: Tyler Heisler-Taylor, Richard Wan, Elizabeth G. Urbanski, Sumaya Hamadmad, Mohd Hussain Shah, Hailey Wilson, Julie Racine, Colleen M. Cebulla.

References

1. Romano C, Price MT, Almli T, Olney JW. Excitotoxic neurodegeneration induced by deprivation of oxygen and glucose in isolated retina. Invest Ophthalmol Vis Sci. 1998; 39(2):416–23. PMID: 9478002
2. Campbell WA, Blum S, Reske A, Hoang T, Blackshaw S, Fischer AJ. Cannabinoid signaling promotes the de-differentiation and proliferation of Muller glia-derived progenitor cells. Glia. 2021. https://doi.org/10.1002/glia.24056 PMID: 34231253
3. Campbell WA, Fritsch-Kelleher A, Palazzo I, Hoang T, Blackshaw S, Fischer AJ. Midkine is neuroprotective and influences glial reactivity and the formation of Muller glia-derived progenitor cells in chick and mouse retinas. Glia. 2021; 69(6):1515–39. https://doi.org/10.1002/glia.23976 PMID: 33569849

4. Lucas DR, Newhouse JP. The toxic effect of sodium L-glutamate on the inner layers of the retina. AMA Arch Ophthalmol. 1957; 58(2):193–201. https://doi.org/10.1001/archopht.1957.00940010205006 PMID: 13443577

5. Olney JW. The toxic effects of glutamate and related compounds in the retina and the brain. Retina (Philadelphia, Pa. 1982; 2(4):341–59. PMID: 6152914

6. Rothman SM, Olney JW. Glutamate and the pathophysiology of hypoxic—ischemic brain damage. Ann Neurol. 1986; 19(2):105–11. https://doi.org/10.1002/ana.410190202 PMID: 2421636

7. Sucher NJ, Lipton SA, Dreyer EB. Molecular basis of glutamate toxicity in retinal ganglion cells. Vision research. 1997; 37(24):3483–93. https://doi.org/10.1016/S0042-6989(97)00047-3 PMID: 9425525

8. Hahn JS, Aizenman E, Lipton SA. Central mammalian neurons normally resistant to glutamate toxicity are made sensitive by elevated extracellular Ca2+: toxicity is blocked by the N-methyl-D-aspartate antagonist MK-801. Proceedings of the National Academy of Sciences of the United States of America. 1988; 85(17):6556–60. https://doi.org/10.1073/pnas.85.17.6556 PMID: 2901101

9. Shen Y, Liu XL, Yang XL. N-methyl-D-aspartate receptors in the retina. Mol Neurobiol. 2006; 34 (3):163–79. https://doi.org/10.1385/MN:34:3:163 PMID: 17308350

10. Dong XX, Wang Y, Qin ZH. Molecular mechanisms of excitotoxicity and their relevance to pathogenesis of neurodegenerative diseases. Acta Pharmacol Sin. 2009; 30(4):379–87. https://doi.org/10.1038/aps.2009.24 PMID: 19343058

11. Kuehn S, Rodust C, Stute G, Grotegut P, Meiner W, Reinehr S, et al. Concentration-Dependent Inner Retina Layer Damage and Optic Nerve Degeneration in a NMDA Model. J Mol Neurosci. 2017; 63(3–4):283–99. https://doi.org/10.1007/s12031-017-0978-x PMID: 28963708

12. Connaughton V. Glutamate and Glutamate Receptors in the Vertebrate Retina. In: Kolb H, Fernandez E, Nelson R, editors. Webvision: The Organization of the Retina and Visual System. Salt Lake City (UT)1995.

13. Wisely CE, Sayed JA, Tamez H, Zelinka C, Abdel-Rahman MH, Fischer AJ, et al. The chick eye in vision research: An excellent model for the study of ocular disease. Progress in Retinal and Eye Research. 2017; 61:72–97. https://doi.org/10.1016/j.preteyeres.2017.06.004 PMID: 28668352

14. Smith SB. Diabetic retinopathy and the NMDA receptor. Drug News Perspect. 2002; 15(4):226–32. https://doi.org/10.1358/dnp.2002.15.4.840055 PMID: 12677206

15. Ishikawa M. Abnormalities in Glutamate Metabolism and Excitotoxicity in the Retinal Diseases2013. 528940 p.

16. Fu RY, Shen QY, Xu PF, Luo JJ, Tang YM. Phagocytosis of Microglia in the Central Nervous System Diseases. Molecular Neurobiology. 2014; 49(3):1422–34. https://doi.org/10.1007/s12035-013-8620-6 PMID: 24395130

17. Mey J, Thanos S. Development of the visual system of the chick. I. Cell differentiation and histogenesis. Brain Res Brain Res Rev. 2000; 32(2–3):343–79. https://doi.org/10.1016/s0165-0173(99)00022-3 PMID: 10760548

18. Thanos S, Mey J. Development of the visual system of the chick. II. Mechanisms of axonal guidance. Brain Res Brain Res Rev. 2001; 35(3):205–45. https://doi.org/10.1016/s0165-0173(01)00049-2 PMID: 11423155

19. Bueno JM, Giakoumaki A, Gualda EJ, Schaeffel F, Artal P. Analysis of the chicken retina with an adaptive optics multiphoton microscope. Biomed Opt Express. 2011; 2(6):1637–48. https://doi.org/10.1364/BOE.2.001637 PMID: 21698025

20. Headington K, Choi SS, Nickla D, Doble N. Single cell imaging of the chick retina with adaptive optics. Current eye research. 2011; 36(10):947–57. https://doi.org/10.3109/02713683.2011.587934 PMID: 21950701

21. Kram YA, Mantey S, Corbo JC. Avian cone photoreceptors tile the retina as five independent, self-organizing mosaics. PLoS One. 2010; 5(2):e8992. https://doi.org/10.1371/journal.pone.0008992 PMID: 20126550

22. Henderson M. Evolution's Witness: How Eyes Evolved. Library Journal. 2011; 136(20):146-.

23. Slijkerman RW, Song F, Astuti GD, Huynen MA, van Wijk E, Stieger K, et al. The pros and cons of vertebrate animal models for functional and therapeutic research on inherited retinal dystrophies. Prog Retin Eye Res. 2015; 48:137–59. https://doi.org/10.1016/j.preteyeres.2015.04.004 PMID: 25936606

24. Weller C, Lindstrom SH, De Grip WJ, Wilson M. The area centralis in the chicken retina contains efferent target amacrine cells. Vis Neurosci. 2009; 26(2):249–54. https://doi.org/10.1017/S0952523808080917 PMID: 19296862

25. Fischer AJ, Seltner RL, Poon J, Stell WK. Immunocytochemical characterization of quisqualic acid- and N-methyl-D-aspartate-induced excitotoxicity in the retina of chicks. J Comp Neurol. 1998; 393(1):1–15. PMID: 9520096

26. Fischer AJ, Seltner RL, Stell WK. N-methyl-D-aspartate-induced excitotoxicity causes myopia in hatched chicks. Can J Ophthalmol. 1997; 32(6):373–7. PMID: 9363340

27. Nickla DL, Wildsoet C, Wallman J. The circadian rhythm in intraocular pressure and its relation to diurnal ocular growth changes in chicks. Exp Eye Res. 1998; 66(2):183–93. https://doi.org/10.1006/exer.1997.0425 PMID: 9533844

28. Ostrin LA, Liu Y, Choh V, Wildsoet CF. The role of the iris in chick accommodation. Invest Ophthalmol Vis Sci. 2011; 52(7):4710–6. https://doi.org/10.1167/iovs.10-6819 PMID: 21357397

29. Schmid KL, Hills T, Abbott M, Humphries M, Pyne K, Wildsoet CF. Relationship between intraocular pressure and eye growth in chick. Ophthalmic and Physiological Optics. 2003; 23(1):25–33. https://doi.org/10.1046/j.1475-1313.2003.00085.x PMID: 12535054

30. Wahl C, Li T, Howland HC. Intraocular pressure fluctuations of growing chick eyes are suppressed in constant light conditions. Exp Eye Res. 2016; 148:52–4. https://doi.org/10.1016/j.exer.2016.05.018 PMID: 27223608

31. Ostrin LA, Wildsoet CF. A Comparison of Applanation and Rebound Tonometers in Young Chicks. Current eye research. 2021; 46(1):71–7. https://doi.org/10.1080/02713683.2020.1782942 PMID: 32618481

32. Heisler-Taylor T, Kim B, Reese AY, Hamadmad S, Kusibati R, Fischer AJ, et al. A new multichannel method quantitating TUNEL in detached photoreceptor nuclei. Experimental Eye Research. 2018. https://doi.org/10.1016/j.exer.2018.06.028 PMID: 29959928

33. McCulloch DL, Marmor MF, Brigell MG, Hamilton R, Holder GE, Tzekov R, et al. ISCEV Standard for full-field clinical electroretinography (2015 update). Doc Ophthalmol. 2015; 130(1):1–12. https://doi.org/10.1007/s10633-014-9473-7 PMID: 25502644

34. Shen Y, Luo X, Liu S, Shen Y, Nawy S, Shen Y. Rod bipolar cells dysfunction occurs before ganglion cells loss in excitotoxin-damaged mouse retina. Cell Death Dis. 2019; 10(12):905. https://doi.org/10.1038/s41419-019-2140-x PMID: 31787761

35. Calvo E, Milla-Navarro S, Ortuno-Lizaran I, Gomez-Vicente V, Cuenca N, De la Villa P, et al. Deleterious Effect of NMDA Plus Kainate on the Inner Retinal Cells and Ganglion Cell Projection of the Mouse. Int J Mol Sci. 2020; 21(5). https://doi.org/10.3390/ijms21051570 PMID: 32106602

36. Chen J, Chiang C-W, Zhang H, Song S-K. Cell Swelling Contributes to Thickening of Low-Dose N-methyl-D-Aspartate–Induced Retinal Edema. Investigative Ophthalmology & Visual Science. 2012; 53(6):2777–85. https://doi.org/10.1167/iovs.11-8827 PMID: 22467578

37. Nishimura T, Machida S, Tada A, Oshida E, Muto T. Macular function following intravitreal ranibizumab for macular edema associated with branch retinal vein occlusion. Doc Ophthalmol. 2019; 139(1):67–74. https://doi.org/10.1007/s10633-019-09696-5 PMID: 30980231

38. Gardasevic Topcic I, Sustar M, Brecelj J, Hawlina M, Jaki Mekjavic P. Morphological and electrophysiological outcome in prospective intravitreal bevacizumab treatment of macular edema secondary to central retinal vein occlusion. Doc Ophthalmol. 2014; 129(1):27–38. https://doi.org/10.1007/s10633-014-9445-y PMID: 24906869

39. Leozappa M, Ferrari TM, Grossi T, Pace V, Rinaldi ML, Battista D, et al. Prognostic prediction ability of postoperative multifocal ERG after vitrectomy for diabetic macular edema. European journal of ophthalmology. 2008; 18(4):609–13. https://doi.org/10.1177/112067210801800418 PMID: 18609483

40. Fu YD, Wang P, Meng XX, Du ZD, Wang DB. Structural and functional assessment after intravitreal injection of ranibizumab in diabetic macular edema. Documenta Ophthalmologica. 2017; 135(3):165–73. https://doi.org/10.1007/s10633-017-9604-z PMID: 28756595

41. Fischer AJ, Seltner RL, Stell WK. Opiate and N-methyl-D-aspartate receptors in form-deprivation myopia. Vis Neurosci. 1998; 15(6):1089–96. https://doi.org/10.1017/s0952523898156080 PMID: 9839973

42. Fischer AJ, Zelinka C, Milani-Nejad N. Reactive Retinal Microglia, Neuronal Survival, and the Formation of Retinal Folds and Detachments. Glia. 2015; 63(2):313–27. https://doi.org/10.1002/glia.22752 PMID: 25231952

43. Veruki ML, Zhou Y, Castilho A, Morgans CW, Hartveit E. Extrasynaptic NMDA Receptors on Rod Pathway Amacrine Cells: Molecular Composition, Activation, and Signaling. J Neurosci. 2019; 39(4):627–50. https://doi.org/10.1523/JNEUROSCI.2267-18.2018 PMID: 30459218

44. Zhou Y, Tencerova B, Hartveit E, Veruki ML. Functional NMDA receptors are expressed by both AII and A17 amacrine cells in the rod pathway of the mammalian retina. J Neurophysiol. 2016; 115(1):389–403. https://doi.org/10.1152/jn.00947.2015 PMID: 26561610

45. Tung NN, Morgan IG, Ehrlich D. A quantitative analysis of the effects of excitatory neurotoxins on retinal ganglion cells in the chick. Vis Neurosci. 1990; 4(3):217–23. https://doi.org/10.1017/s0952523800003369 PMID: 2078503

46. Barrington M, Sattayasai J, Zappia J, Ehrlich D. Excitatory amino acids interfere with normal eye growth in posthatch chick. Current eye research. 1989; 8(8):781–92. https://doi.org/10.3109/02713688909000868 PMID: 2676355

47. Sattayasai J, Zappia J, Ehrlich D. Differential effects of excitatory amino acids on photoreceptors of the chick retina: an electron-microscopical study using the zinc-iodide-osmium technique. Vis Neurosci. 1989; 2(3):237–45. https://doi.org/10.1017/s0952523800001152 PMID: 2487650

48. Lebrun-Julien F, Duplan L, Pernet V, Osswald I, Sapieha P, Bourgeois P, et al. Excitotoxic death of retinal neurons in vivo occurs via a non-cell-autonomous mechanism. J Neurosci. 2009; 29(17):5536–45. https://doi.org/10.1523/JNEUROSCI.0831-09.2009 PMID: 19403821

49. Wali N, Leguire LE. The photopic hill: a new phenomenon of the light adapted electroretinogram. Doc Ophthalmol. 1992; 80(4):335–45. https://doi.org/10.1007/BF00154382 PMID: 1473449

50. Rufiange M, Dassa J, Dembinska O, Koenekoop RK, Little JM, Polomeno RC, et al. The photopic ERG luminance-response function (photopic hill): method of analysis and clinical application. Vision research. 2003; 43(12):1405–12. https://doi.org/10.1016/s0042-6989(03)00118-4 PMID: 12742110

51. Rufiange M, Rousseau S, Dembinska O, Lachapelle P. Cone-dominated ERG luminance-response function: the Photopic Hill revisited. Doc Ophthalmol. 2002; 104(3):231–48. https://doi.org/10.1023/a:1015265812018 PMID: 12076014

52. Hamilton R, Bees MA, Chaplin CA, McCulloch DL. The luminance-response function of the human photopic electroretinogram: a mathematical model. Vision research. 2007; 47(23):2968–72. https://doi.org/10.1016/j.visres.2007.04.020 PMID: 17889925